

# Review on surface characteristics of components produced by direct metal deposition process

S. Pratheesh Kumar\*, K. Anand, S. Hari Chealvan and S. Karthikeya Muthu

Department of Production Engineering, PSG College of Technology, Coimbatore, Tamil Nadu-641004, India  
Phone: +91 9489227914; Fax.: 04222592277

**ABSTRACT** – Direct metal deposition is a metal additive manufacturing process that builds objects layer by layer. The surface properties of direct metal deposition components are discussed in this study. The fluctuation of surface attributes such as roughness, finish, texture, and so on as a function of operation parameters has been investigated for a number of materials. This research assists in identifying the optimal process parameters for the material chosen, such as material feed rate, gas flow rate, and laser power, in order to generate the best surface characteristics. The results show that wire feed deposition surpasses powder feed deposition. The laser power and scanning speed of the laser were found to be the most influential process parameters. The study results reveal that the optimum process parameter combinations are material specific and is the keyfactor for obtaining better products with reduced surface roughness and waviness. The microstructural study also explores the material specific effect in process parameter combinations. This research could be used to determine or predict the best process parameters for a wide range of industrial materials.

## ARTICLE HISTORY

Received: 17<sup>th</sup> June 2022

Revised: 04<sup>th</sup> Nov. 2022

Accepted: 29<sup>th</sup> Oct. 2022

Published: 27<sup>th</sup> Dec. 2022

## KEYWORDS

Additive manufacturing

Direct metal deposition

Surface characteristics

Surface roughness

Surface waviness

## INTRODUCTION

Rapid prototyping is the process of rapidly building a replica of a real system or component prior to its final release or commercialization in a range of industries. In other words, the emphasis is on rapid creation of anything, with the result being a prototype or basic model from which further models and, eventually, the final product can be produced [1,2]. The components in RP technology are manufactured by an additive process. The American Society for Testing and Materials international's newly formed technical committee decided on the adoption of new nomenclature. The term AM appears in the recently adopted ASTM consensus [3]. The primary idea behind this technology is that a 3D CAD model can be generated instantly without the requirement for production planning. Parts are created by layering material; each layer may be a smaller cross-section of the component obtained from the basic CAD data [4]. "Laser powder deposition," "laser metal deposition (LMD)," "laser material deposition," "laser-aided direct metal deposition (DMD)," "laser-based multi-directional metal deposition", "laser engineered net shaping (LENS)" or "digital light fabrication (DLF)", and "LMD shaping" are all terms used to describe the DMD technique [5]. Direct energy deposition (DED) is a type of additive manufacturing (AM) technique that may be used to both repair and create new 3D items [6]. The DMD approach's adaptability allows for the simultaneous use of various materials, making it excellent for the fabrication of functionally graded components [7]. As a result, it offers flexibility and the potential to significantly reduce the by-to-fly ratio, particularly in the aviation industry. This critical AM technology has also been certified for use in a variety of industries, including aerospace, automotive, and medical [8,9].

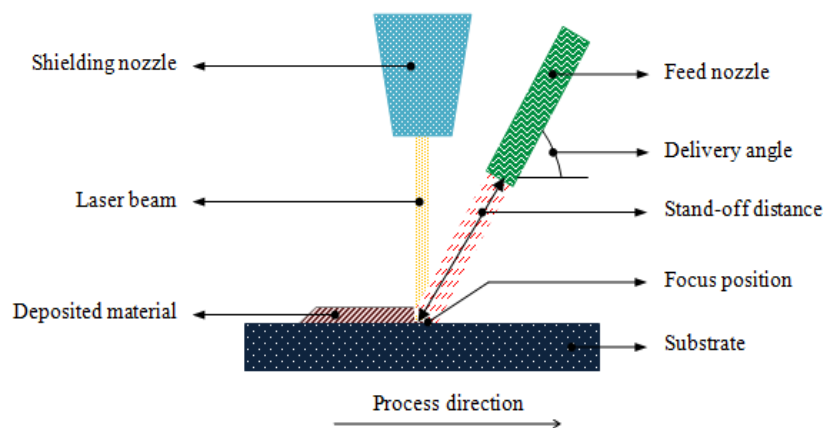


Figure 1. Direct metal deposition process

As shown in Figure 1, the DMD process is carried out by continuously feeding material feedstock into the molten laser focal area on the substrate, thereby forming a melt-pool throughout the substrate [10]. The DMD method uses a laser's coherence and directionality features to produce a melt pool on the surface of the substrate as the beam hits at it. This melt-pool takes in wire or powder as input and melts it. The establishment of this melt-pool results in the formation of a solid track of the deposited material, which can be seen following the laser beam. Various material feedstocks are placed in multiple powder feeding hoppers or wire feeders when developing composite materials or functionally graded materials, and the materials are delivered concurrently or sequentially to develop the composite, with the material composition chosen based on its location within the component via coaxial nozzles located next to the laser source [10]. Figure 2 exhibits a flow chart depicting the various stages required in producing a part utilising DMD technology.



Figure 2. Steps in DMD process

## MATERIAL FEEDING MECHANISM

DMD technology is divided into two variations that help with the fabric feeding method used to manufacture the parts. Powder-fed and wire-fed systems are both available [11].

### Powder Feeding

In the powder feed system depicted in Figure 3(a), metallic powder is delivered or sprayed onto the laser-generated melt pool on the substrate surface. In the melt pool, the powder melts and solidifies. A structural metal with a high melting point, a binder metal with a low melting point, and trace amounts of additives such as a fluxing agent or deoxidizer are often included in the powder mixture. This results in a clad track, which can subsequently be used as a basis for additional deposition, resulting in a three-dimensional object. Metallic powder blends have been investigated as a method of synthesising alloyed components or functionally graded structures from elemental powders. The disadvantages of the technology include the low deposition rate, difficulty in maintaining a high catchment efficiency, and the commonly produced poor quality surface finish [10,12].

### Wire Feeding

Metallic powders are often used in DMD techniques to make things with near-net form. Wire feeding is also employed in laser cladding and material addition applications. Both powder and wire feed laser deposition have advantages and downsides. Wire feeding laser deposition is frequently faster and uses more material than powder feeding laser deposition [13]. In wire feeding, the wire is typically provided from one side, as seen in Figure 3(b). New commercial laser cladding heads coaxially feed the wire and divide the laser into numerous distinct beams that focus on a circular focal point. As a result, omnidirectional deposition is a viable option. Side feeding of the wire challenges path planning since the wire should always be fed at the leading edge of the melt pool to achieve the best surface roughness and porosity output [14].

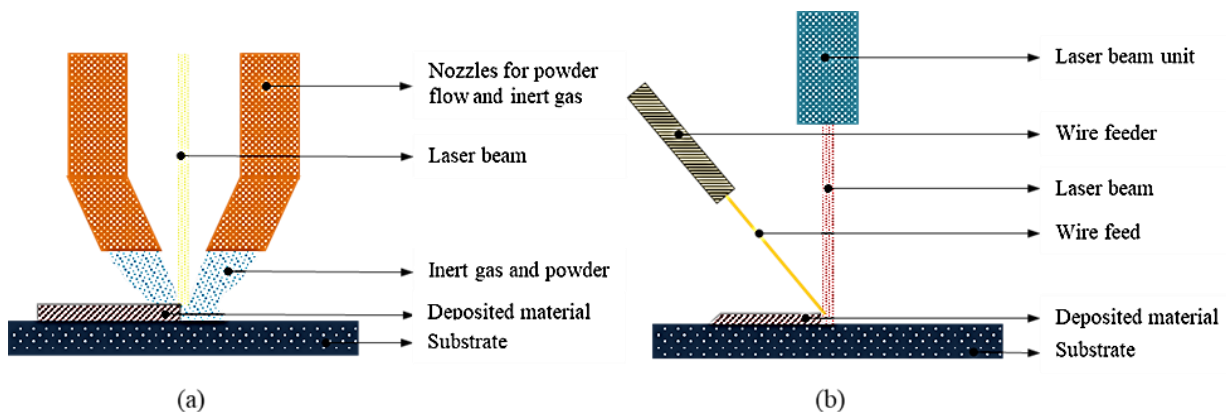


Figure 3. Material feeding mechanism: (a) powder and (b) wire

## PROCESS PARAMETERS

The DMD method enables the control of surface attributes such as roughness, hardness, and polish on produced parts. These characteristics are inextricably linked to microstructural change. Microstructure evolution is determined by the rate of solidification or cooling, and connections exist between process parameters and those factors [14].

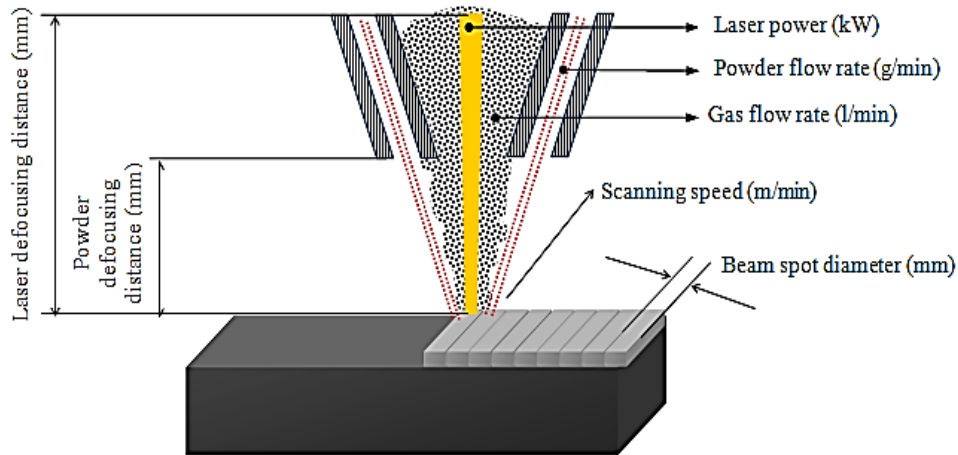


Figure 4. Process parameters in DMD

### Laser Power

As illustrated in Figure 4, laser power is the amount of heat energy created by the laser and used in material processing. Dilution occurs when the laser power is too high, which is undesirable in the DMD process since it affects the component's geometrical accuracy. It is highly sensitive to process stability, which remains an issue in the DMD process. As the laser power increases, the porosity and dimensions of the porosity decrease. The laser power had a substantial effect on both the dilution level and the surface roughness created. While dilution is required for good bonding between the substrate and the deposited powder, excessive dilution is not. Dilution increases as laser power increases, although surface roughness decreases [15]. When the substrate and depositing material are same, surface hardness increases with travel speed but decreases with laser power and powder particle size. Because these parameter changes result in increased cooling rates, the yield and tensile strengths of the deposited material typically rise with travel speed and decrease with laser power [15].

### Scanning Speed

The term "scanning speed" is often used to refer to the pace at which a beam is fed [16]. As illustrated in Figure 4, this value indicates the duration of the laser's interaction with the deposited material and substrate. The scanning speed is increased in the DMD process by either moving the laser source against a substrate attached to a stationary building platform or by moving a substrate on a CNC five-axis table against a fixed laser head [17]. Scanning speed is a critical component that can affect the quality of the final result. As the scanning speed increases, the width of the single-track cladding layer decreases, and the track height is dictated by the scanning speed [18]. Scanning speed has an effect on the form, degree of porosity, and size of the component. As the scanning speed drops, the quantity of porosity reduces. When compared to the influence of laser power, scanning speed had a significant effect on the degree of porosity. By utilising a sufficient laser power and increasing the scanning speed, it was possible to maintain the molten pool temperature throughout the operation, resulting in an improved surface finish [19].

### Powder Defocusing Distance

The form of the laser point changes as the particle defocusing distance increases during the procedure, as illustrated in Figure 4. Variation in powder defocusing distance has a noticeable effect on the surface quality of the part. The effect of powder defocus distance on layer quality is significant because it impacts the overlap rate, which affects the surface flatness. The surface flatness of the cladding layer decreases initially and subsequently increases as the defocusing distance increases. There is no obvious difference when the defocusing distance is closer to the focus point. The powder defocusing distance has an effect on the hardness of the layer. The hardness of the cladding layer increases initially and subsequently decreases as the defocusing distance increases, reaching a maximum at the focus point when the defocusing distance is negative. When the defocusing distance is close to the focus point, the microstructure of the cladding layer acts normally, but there is some change in the microstructure during the defocusing stage. To summarise, particle defocusing below the substrate can improve the quality of the surface [18,20].

## Laser Defocusing Distance

The diagram in Figure 4 illustrates a schematic representation of the laser defocusing distance.  $D_f > 0$  indicates the laser defocusing distance when the work plane of the substrate is above the laser beam's focal plane, and  $D_f < 0$  indicates the laser defocusing distance when the work plane of the substrate is below the laser beam's focal plane [21]. The microstructures became coarser as the absolute value of the laser defocusing distance rose. Because the increased laser defocus distance resulted in a larger molten pool, the size of the molten pool increased. The solidification period of the molten pool increased, the cooling rate reduced, the temperature gradient decreased, the nucleation rate plummeted, and the cellular grains increased in size [22]. The track height lowers first when the laser passes beneath the melt pool and then grows as the distance between the melt pool and the laser focus increases. To summarise, the laser defocusing distance is used above the substrate; it has a negligible effect on the surface quality but has the potential to improve it.

## Powder Flow Rate

The powder flow rate is a crucial determinant in determining the roughness of DMD components, as illustrated in Figure 4 [10]. It refers to the amount of material that exits the delivery nozzle over a specified time period. The average surface roughness ( $R_a$ ) rose as the powder flow rate was increased. To achieve a higher surface quality, it is necessary to maintain a low powder flow rate. When the flow rate of the powder is decreased, the porosity drops. Powder flow velocity appears to be increasing, but dilution depth appears to be decreasing. This is because more powder is available for melting at a quicker powder flow rate, preventing the substrate from melting more than necessary, resulting in excessive dilution. Alternatively, the  $R_a$  appears to grow as the powder flow rate is increased. The explanation for this is that even at low powder flow rates, the available laser power was sufficient to melt the powder, resulting in the observed low surface roughness. Increased surface roughness may be noticed at high powder flow rates as a result of improper melting of deposited powder. The quantity of dilution decreases as the powder flow velocity increases, but the roughness increases. Increases in powder flow rate result in large increases in track width, track height, and deposit weight. The average microhardness increases as the powder flow rate is increased [23].

## Gas Flow Rate

Gas flow rate is another critical LMD process parameter. It relates to the rate at which powder carrier gas flows as shown in Figure 4. The powder material is transported by a carrier gas, which is an inert gas that protects the powder from environmental damage, particularly reactive compounds. However, it has a negligible effect on the resultant properties of the deposited samples. Although it exerts a greater drag force on small particles, when the particle size dispersion is significant, the small particles are clearly concentrated in the centre of the focal powder area, while the perimeter is scattered with large powder [24]. Due to the fact that a higher gas flow rate results in a greater drag force on particles, powder separation can occur considerably more quickly and visibly. Apart from that, the intersection point of the powder volume percentages showed earlier and earlier as the argon gas flow rate increased. As a result, powder separation happened far more quickly than with a lower argon gas flow rate [25].

## Beam Spot Diameter

The diameter of a laser beam measured at a certain focal distance is referred to as the beam spot diameter, as illustrated in Figure 4. The diameter of the laser point has a significant effect on the energy density in the DMD process [22,23]. When the size of the wall exceeds the dimensions of the heat source, this is most likely due to the tiny diameter of the laser point. Due to the fact that the width of the material stream is frequently more than the diameter of the melt pool, the longer the laser defocusing distance, the larger the laser spot size, resulting in more powder entering the melt pool and a greater building height. A large laser spot diameter can result in a large molten pool, which can result in powder being infused into the melt pool. Additionally, because the track height increases, a large laser spot diameter can result in a decrease in beam power density, which can result in sticky powder in the DMD process, affecting part forming quality [18]. When compared to more essential factors such as scanning speed and laser power, the diameter of the laser spot is a minor factor in surface polishing. It does, however, have an effect on the surface quality, which can result in a more polished finish [23,24]. Additionally, it is observed that the diameter of the beam spot is the most critical factor in determining the initial track width on the substrate, given that the absorbed heat flux is sufficient to promote melting [24,25].

## Laser Pulse Frequency

The number of cycles produced during a unit time interval, as seen in Figure 5, is referred to as the pulse frequency. As the number of cycles per second grows, the duration of on-time decreases [26]. The operator has greater control over the energy supply when utilising a pulse laser, which has a significant effect on the solidification of the molten pool and subsequent component manufacturing. The difference in hardness between the edge and the central region changes significantly depending on the pulse laser settings. The part produced using a pulse laser has a greater ultimate tensile strength (UTS) than the part produced using a continuous wave laser (CWL) [27]. While a pulsed beam can reduce the

porosity of a continuous beam, the low repetition frequency of the pulses results in a coarse layer structure. Surface roughness is not much affected by pulse frequency, although it is improved when the laser is operated in pulsed mode rather than continuous wave mode. The component's hardness increases as the frequency of the pulses increases and is frequently greater in the middle of the wall than at the top levels. To summarise, pulsed beams can be used to fabricate consolidated components suitable for functional prototype and tooling applications, and the laser pulse frequency has an effect on the final characteristics of the part [28,29].

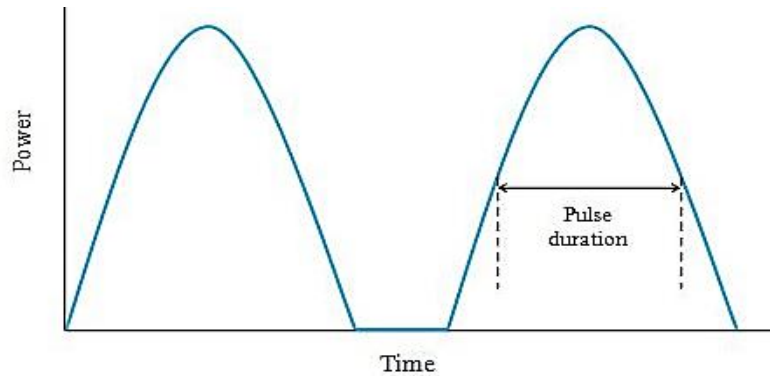


**Figure 5.** Laser pulse frequency

### Shape of Laser Beam

The laser beam shape can be majorly classified into two types, are solid and annular. With a solid laser beam with Gaussian distribution, the scanning energy intensity was greatest at the centre and decreased toward the border, as seen in Figure 6(a), which could result in overheating at the centre and insufficient melting at the edge. By comparison, typical solid Gaussian laser irradiation generated the lowest temperature near the molten pool's edge, which was insufficient to totally melt powder particles. Although increased scanning speeds may increase tiny waviness, ordinary solid Gaussian laser irradiation has a minor effect on surface roughness.

A collimated beam is formed into an annular laser beam using a laser beam shaping apparatus, as seen in Figure 6(b). The annular laser spot is then transferred coaxially along the axis of the material delivery tube and onto the focusing device, where it is focused onto the workpiece surface by the mirror. By and large, employing an annular laser beam with an axially fed material increases the symmetry of the deposition process, which benefits its stability and robustness [30]. SS 316 coatings utilising a ring-shaped laser spot and discovered that when a ring-shaped beam was used rather of a Gaussian beam, the microstructure was clearly finer. Nano diamond coatings on aluminium alloy A319 substrates with an annular beam were shown to have superior surface finish and tribological features than those with a Gaussian beam [31]. An annular laser beam generates a higher temperature at the margins and a smaller thermal gradient, which may aid the DMD process in improving the finish of thin walls.

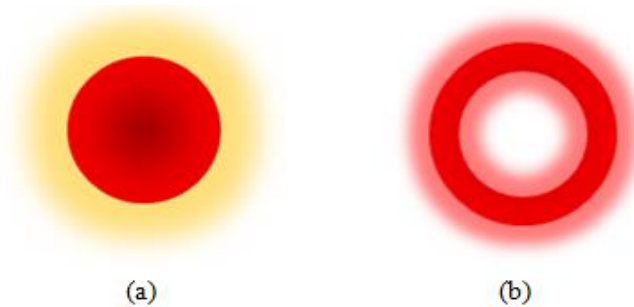


**Figure 6.** Shape of laser beam spot: (a) solid and (b) annular

### SURFACE CHARACTERISTICS

The qualitative characteristics of surface integrity parameters include shape, topography, hardness, contamination, residual stress, and microstructure [32]. Additionally, recent focus has been paid to the surface properties of fabricated goods, which include surface roughness, surface texture, corrosion resistance, and waviness [33].

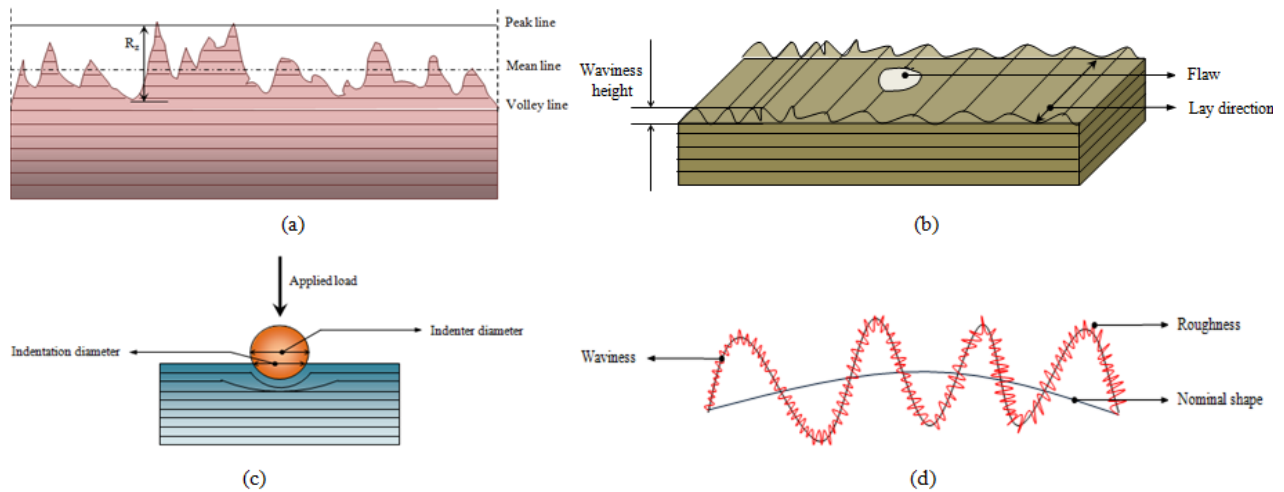


**Figure 7.** Surface characteristics: (a) surface roughness parameters, (b) surface finish parameters, (c) surface hardness and (d) surface topography components

### Surface Roughness

The arithmetic mean is a commonly used measure for calculating the roughness of a surface. It is calculated from the profile's mean line. If the unpredictability of the roughness level is greater than that of the peak's top, the highest peak of  $R_{\max}$  or the maximum height of  $R_z$  must be measured. The roughness profile's parameters are defined in detail in Figure 7(a) [34,35]. When the deposition direction is 90 degrees, a higher roughness is obtained [36]. Surface roughness characteristics were shown to benefit from layer thickness reduction while simultaneously boosting melt-pool volume to facilitate remelting operations. High interaction distances, which correlate to the time-of-flight of molten powder particles, encourage low  $R_t$  roughness. When the laser power is high, roughness characteristics are often lowered [37]. The roughness height and width decrease as the scanning speed increases. Due to the rapid scanning speed of the laser beam, the copper powder has an excellent surface roughness.

### Surface Finish

Due to the low surface finish of DMD, as illustrated in Figure 7(b), components must be machined to meet geometrical and mechanical (fatigue) strength requirements. Both the AM process's layer-by-layer structure (staircase effect) and powder particles adhering to the surface contribute to poor surface quality. Both factors are influenced by process parameters, part geometrical features, and powder properties. A higher laser power can result in more efficient melting of the deposited material and a flatter surface. Increased laser power during the DMD process can result in a bigger melt pool, which can improve the surface quality of deposited samples. By locating the powder focus below the melt-pool, the melt-pool is enhanced, resulting in the finest possible surface finish. Combining low scanning speed and high laser power results in a higher surface quality. The surface smoothness is increased by utilising thinner additive layers and larger melt pools, as well as by increasing the distance between powder or laser interaction points, which results in particle melting [37]. Increase the scanning speed, melt-pool size, and temperature control to increase the surface finish [38].

### Surface Waviness

The waviness of the items' treated surfaces, as well as their roughness and shape accuracy, all have a substantial effect on their service reliability [39]. As seen in Figure 7(b), waviness is a surface imperfection with a wavelength larger than the roughness [40]. Alternatively, surface waviness refers to low frequency imperfections on a surface that are overlaid with surface roughness [41]. The surface of the DMD produced part contains macro and micro geometrical features. The macro one is the waviness of the surface caused by layer-by-layer deposition direction. Adjust the pulse energy, scanning speed, and pulse frequency to decrease surface waviness. Increased pulse energy alleviates surface waviness [42]. Periodic menisci were the major factor affecting surface finish, contributing to macroscopic waviness. Additionally, the valley between two neighbouring layers and the wave that exists for only one layer contribute macroscopically to the macroscopic waviness ( $W_t$ ). It can be significantly improved by increasing the scanning speed.

### Surface Hardness

The hardness of a material is determined by its intrinsic hardness, as seen in Figure 7(c), which is the hardness of the material in single crystal form, as well as its microstructural nature, which affects deformation mechanisms. As the rate of cooling increases during solidification, the hardness increases. Additionally, as traversal speed increases, so does the surface hardness of deposited layers. Due to the three-dimensional heat flow near the substrate, high hardness values are

obtained, but subsequent layer deposition results in low values due to re-heating. Surface hardness is affected by laser power, traverse speed, and particle size. Hardness increased with traverse speed, but decreased with laser power and powder particle size. The increased hardness values are mostly due to the smaller grain size present in DMD manufactured parts [43]. Microhardness of deposition rises with increasing scanning speed. The laser region's microhardness value was increased following heat treatment [44]. The microhardness of the substrate increases from the cross-section to the upper surface. Grain refinement increases microhardness [45].

### Surface Topography

The surface topography of the material has a direct effect on the wetting, spreading, and moistening attitude of the in-contact fluid. Microorganisms' colonisation is influenced by surface topography, as illustrated in Figure 7(d). It varies according to the angle at which DMD pieces are assembled [46]. 3D and 2D roughness analyses are used to determine the topography of the surface. Due to the fact that the surface topography reflects the amount of fluid filled during the production process and the size of the melt pool, the deposition quality may be improved if the surface topography is stable and has fewer surface faults. The surface of the molten pool oscillated due to the effect of flow fields and temperature, and the topography of the surface could be uneven after solidification. The quantity of shielding gas flow rate and scanning speed are two process parameters that affect the surface topography of a formed layer [47].

### Surface Defects

DMD is a complicated AM method that entails numerous procedures. However, it is associated with a considerable risk of failure due to the probability of defect creation. If not recognized in a timely manner, it might result in considerable losses [48]. There are several number of surface defects are occurred in DMD produced part, but majorly occurred as cracks, lack of fusion and gas porosity.

Cracks are a leading cause of component failure, resulting in the disposal of high-value components. As illustrated in Figure 8(a), small cracks can be seen surrounding the fusion area when the component is fixed with DMD. These strains would be caused by thermal contraction during the rapid cooling period [49]. Cracks form in the interdendritic zones due to the chemical composition of the powder. When combined with high quantities of sulphur, phosphorus, and silicon, a high nitrogen content may increase the susceptibility to cracking [50]. Despite modifying the scanning speed to control cooling rates, cracks in claddings on substrates at ambient temperature were detected as a result of stresses caused by a thermal differential between the substrate and the deposited layers. Using substrate preheating, the gradients were efficiently controlled, resulting in crack-free multilayer deposition [51]. In the DMD, the cladding layer may have macro- and micro-cracks. The former are solidification cracks, which are typically (hot) cracks that begin near the solidification temperature. They are caused by a deficiency of liquid metal replenishment as a result of the consolidation and contraction processes rapidly releasing stress in response to increasing thermal stress generated by rapid cooling.

As illustrated in Figure 8(b), flaws with irregular, elongated shapes ranging in size from 50  $\mu\text{m}$  to several millimetres are classed as lacking fusion. Inadequate overlap between passes results in fusion faults, which are exacerbated by a mismatch in the hatch spacing parameters, which define the space between two consecutive passes [52]. If the powder feed rate is too slow, the desired height may not be achieved; if it is too fast, not all powder particles may melt, resulting in the absence of fusion at the layer interface [53]. Inadequate fusion results in weakened metallurgical bonds and imperfections such as interlayers or pores in the beads, resulting in low perpendicular elongation and UTS. To achieve an appropriate bead form, it is necessary to minimise the effect of gas pressure and to avoid fusion failure [54]. Increased laser power, slower traverse speed, or thinner layers all contribute to the promotion of fusion and the reduction or elimination of void material [55].

As illustrated in Figure 8(c), porosity formation is one of the inherent difficulties associated with DMD using gas assisted powder transfer that may be detrimental to the bulk material's mechanical qualities [56]. The gas porosity increases when the powder feed rate and shielding gas are increased. Gas porosity can be minimised by combining a low powder feed rate with a reduced laser power. When the powder feed rate is high and the laser power is low, the gas porosity increases significantly [57]. The size misfit between the non-spherical and spherical powders enhances the porosity of the laser-melted layer. Increased porosity occurs during DMD as a result of decreased laser absorption and extension of the powder-depleted zone due to lower packing density. While the thickness of the powder layering is significant, a little overlapped area may even cause porosity as a result of insufficient heating of the deposited material. Porosity development during DMD is dependent on the laser processing parameters and powder morphologies. This means that during the DMD process, particle morphologies and operating settings of the laser can actively control porosity [58].

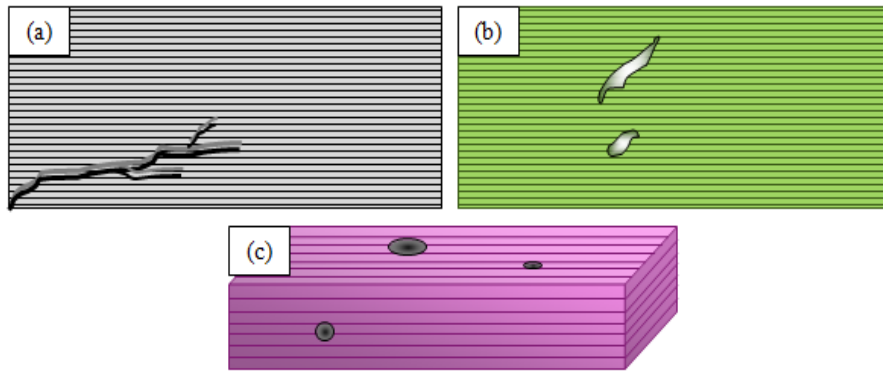


**Figure 8.** Surface defects: (a) cracks, (b) lack of fusion and (c) gas porosity

### Surface Texture

As illustrated in Figure 9, surface texture refers to the geometric irregularities present on the surface. Surface texture does not include mathematical irregularities that aid in the contour or shape of the surface. The shape and size of the powder particles have an effect on the surface texture of the formed layers [59]. Parts are deposited to a tenth of a micrometre arithmetic  $R_a$ , necessitating an additional polishing step for certain applications that require great precision and a delicate surface texture. Under this approach, the texture and surface quality of the powder passage are vital, and polishing is required to produce the desired surface finishes [60]. The texture strength is expected to diminish as the cooling rate increases, enabling the martensitic transition. This exemplifies the critical nature of cooling rate. Consequently, attempting to control the rate of cooling of AM parts could afford significant potential for microstructure adjustment and thus texture control [61].

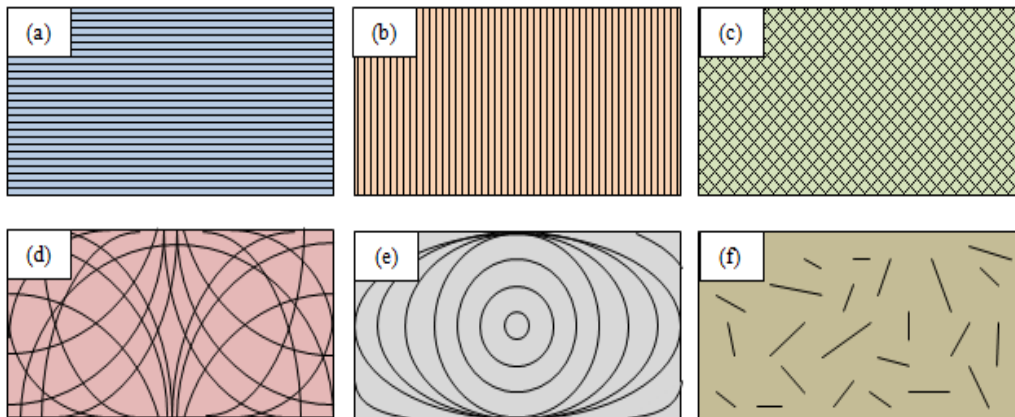


**Figure 9.** Surface texture patterns: (a) parallel, (b) perpendicular, (c) diagonal, (d) multi, (e) circular and (f) isotropic

### Microstructure

As illustrated in Figure 10, the microstructure progression during the manufacturing process is significantly different than that of conventional casting and welding, owing to the significantly faster cooling rate, highly non-equilibrium state, cyclical heating and cooling procedure, and real-time material addition. Because it is directly impacted by the material and manufacturing processes, the as-deposited microstructure plays a key role in establishing a product's mechanical properties [62]. Numerous variables in the DMD process, including laser power, powder flow rate, and scanning speed, can influence the microstructure of a manufactured object [63]. The columnar prior-grains microstructure formed during laser precipitation of Ti6Al4V is dependent on the laser operating settings that control the solidification cooling speeds. However, the dimension of microstructure grains changes as a function of laser energy or indirectly as a result of cooling rates [64]. It is beneficial to develop the ultrafine microstructure during the quick directed solidification process using extremely high temperature gradients, since this results in more uniform component dispersion [65]. The operation parameters are rigorously regulated, resulting in a clad with a uniform thickness and a very fine and controlled microstructure, as well as the possibility to raise the solid solubility of some elements in another [66].

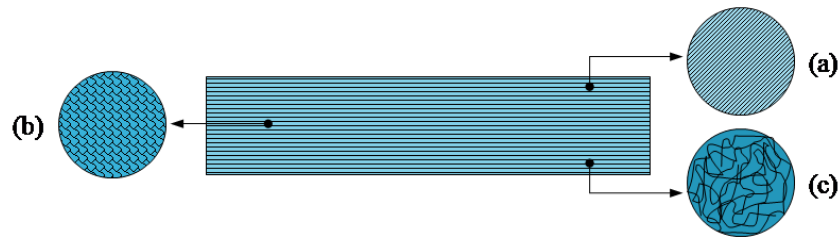


**Figure 10.** Evolution of microstructure at: (a) top layer, (b) middle layer, and (c) bottom layer

DMD is a fascinating and rapidly growing approach with numerous potential applications in industries like as aerospace, medicine, and automotive. The process's fundamentals are investigated. Furthermore, the effect of different input variables on different output variables is studied. Surface attributes of DMD produced components, like those of any other AM technology, are significantly controlled by the input process variables that determine the surface quality of the part. As a result, it is vital to understand how output quality varies in response to changing process parameters for different materials. The following literature review might help you understand how output process parameters change in response to changes in process input elements.

Mahamood and Akinlabi [67] studied the effect of processing factors on the surface quality of titanium alloys generated by LMD. The laser's power has been increased from 0.8 to 3.2 kW. The scanning velocity was set to 0.005 m/s, and the powder flow rate was kept constant at 2 g/min. Similarly, the gas flow rate was held constant at 2 l/min. According to the findings, increasing the laser power reduced the surface roughness, as shown in Table 1. The influence of scanning speed on laser-deposited copper on a titanium alloy substrate was investigated by Erinoshio et al. [34]. The experiments were conducted by increasing the scanning speed to 1.2 m/min from 0.3 m/min while keeping constant laser power, powder feed rate, and gas flow rate. The microstructure and surface roughness of the increasing microstructure of the laser deposited copper were employed to characterise it.  $R_a$  was measured and dropped from 6.70 to 1.41  $\mu\text{m}$  as the scanning speed was increased from 0.3 to 1.2 m/min, as shown in Table 1. Because smaller particle sizes are easier to concentrate, resulting in higher efficiency and larger deposits, the experiments demonstrated that the average particle size has a direct and indirect effect on the deposit height and efficiency for the Inconel 625 utilised. The study's findings, as shown in Table 1, will enable for more informed powder size selection for a number of applications ranging from repair to cladding.

Peyre et al. [68] focused on understanding the physical mechanisms that contribute to poor surface finish and devising a variety of experimental tactics for resolving them. According to the findings, non-melted or partially melted particles adhere to loose surfaces, degrading the surface and resulting in the formation of menisci with different curvature radii. Rombouts et al. [36] examined the effects of surface inclination angle on the surface finish of LMD components and proposed ways for increasing the surface finish. Following powder deposition, laser remelting considerably enhanced the surface quality on both the sides and top surfaces. As seen in Table 1, the surface roughness levels found in this study are significantly lower, which may be due to the filtration of the surface profile data utilised to determine roughness values. Gharbi et al. [37] investigated how key process variables affected the surface finish quality of a titanium alloy (Ti6Al4V) throughout the DMD process. The purpose of this study was to gain a better knowledge of the physical causes of poor surface finishes and to propose some experimental methods for improving them. Surface degradation is dependent on layer thickness drop, as indicated in Table 1, and increasing melt-pool quantities to stimulate remelting processes enhances roughness characteristics.

Chang et al. [31] investigated the impurity concentration, microstructure, and mechanical characteristics of Ti6Al4V blocks deposited in a semi-open environment using a powder-feed annular LMD method. As indicated in Table 1, the results show that in a semi-open environment, annular LMD produced Ti6Al4V can achieve a dazzling silver surface finish and that the quantity of interstitial elements such as oxygen, nitrogen, and hydrogen is much less than the ASTM Grade 5 permissible limits. Wang et al. [49] replicated faults by milling a square groove into the upper surface of each plate of H13 hot work tool steel. Using various combinations of deposition settings, each sample was tested for mass deposition rate, deposition microstructure, signs of porosity, and mechanical qualities such as microhardness and tensile strength. As demonstrated in Table 1, the laser direct metal deposition (LDMD) technique is capable of producing high quality interior fault fixes. The results of each test, however, demonstrate the process's sensitivity to optimal deposition parameter selection. Syed and Li [69] investigated the effect of wire feeding direction, angle, and location on the DMD process for single and multilayered clad or components using a high power diode laser (HPDL). Front feeding and putting the wire close to the leading edge of the melt pool produced the best results in terms of surface finish, geometry control, and sample quality. When rear feeding, the optimal results were obtained by putting the wire at the trailing edge. As seen in Table 1, increasing the angle of feeding increased surface roughness for front feeding while decreased it for rear feeding.

Zhu et al. [18] evaluated the effect on surface quality of rule changes in powder and laser defocusing distance. To accomplish the smooth surface of the parts in laser DMD, three distinct powder defocusing distance conditions were used to make the thin-walled metal components. The experimental results revealed that a good surface quality could be attained by combining a powder targeted below the substrate and a laser aimed above the substrate processes, as shown in Table 1. Mahamood et al. [68] investigated the influence of laser power and powder flow rate on dilution and surface roughness. The powder flow rate was selected to be between 2.88 and 5.76 g/min, and the laser power between 1.8 and 3.0 kW. Both

the scanning speed and the gas flow rate were held constant at 0.05 m/sec and 4 l/min, respectively. According to the research, as laser power increases, so does the degree of dilution, while the Ra value decreases. Table 1 demonstrates that when the powder flow velocity increased, the dilution decreased and the Ra of the surface increased. Pinkerton and Li [28] used the pulse frequency of the laser beam to determine the final wall shape and microstructure of metals deposited in multiple-layer. A pulsed beam microstructural analysis of numerous layers of consolidated 316L steel revealed a coarser but less porous austenitic structure. As shown in Table 1, the steel's final hardness increased as the pulse frequency increased, though not uniformly along the wall, and the surface roughness varied slightly.

Dadbakhsh et al. [70] investigated the use of lasers to clean LMD component surfaces. The LMD process was used to produce a series of Inconel 718 block samples. The top surfaces of the samples were then laser scanned with various parameters. As demonstrated in Table 1, a laser may increase the finishing surface of LMD components to around 2 m Ra, making them acceptable for a wide range of industrial applications. Zhang et al. [19] investigated the effect of a newly developed annular laser beam and laser scanning speed on the surface quality of thin wall parts. The results indicate that the annular laser beam, which generates a higher temperature at the margins than it does in the centre, is advantageous for smoothing surfaces. The surface finish of thin walled products can be significantly improved by increasing the scanning speed of the laser. An annular laser beam with an optimal scanning speed of 8 mm/sec creates an attractive surface polish on thin-wall objects with  $R_a$  of 3  $\mu\text{m}$  and  $W_t$  of 18  $\mu\text{m}$ , as demonstrated in Table 1. Syed et al. [70] investigated a novel deposition process in which powder from a coaxial nozzle and wire from an off-axis nozzle are simultaneously fed into the deposition melt pool. A 1.5 kW diode laser is used to fabricate multilayer parts from 316L steel, and the surface roughness, deposition rate, porosity, and microstructure of numerous powder and wire nozzle designs are compared. Combining the two techniques increased deposition efficiency and decreased surface roughness. The samples obtained using this procedure contain some porosity, albeit it is far less than the porosity found in samples generated solely using powder, as seen in Table 1.

Amine et al. [71] sought to characterise the effect of newly deposited layer laser settings on the microstructure and mechanical properties of previously deposited layers in order to guide future direct laser deposition (DLD) manufacturing parameters selection. The microstructure of the top layer was equiaxed, however the portion near the substrate was fine dendritic. As illustrated in Table 1, both travel speed and laser power have a significant effect on the microstructure and hardness of the sample. Sun et al. [20] evaluated the layer's quality by altering the defocus distance while maintaining constant the other laser cladding process parameters. Additionally, the study evaluated the cladding layer's breadth, height, surface flatness, flat-wide-to-flat-high ratio, hardness, and microstructure. As shown in Table 1, cladding layer surface flatness decreases first and then increases as the defocus distance increases, whereas cladding layer hardness increases initially and subsequently decreases.

Bhardwaj et al. [46] studied the influence of generated surface topography on corrosion and in-vitro bioactivity with the goal of minimising post-fabrication surface modifications. The effect of surface roughness on corrosion resistance is examined in vitro using simulated bodily fluids (SBF). Vertically created samples have a rougher surface than horizontally generated samples, whereas horizontally generated samples have up to 75% higher corrosion resistance as shown in table 1. Syed et al. [71] researched a new technology that combines wire and powder feeding in order to increase production speed and material efficiency while maintaining geometry quality. Utilizing diode laser strengths ranging from 1 kW to 1.5 kW, multilayer products made of 316L stainless steel are created utilising powder feeding, wire feeding, and the combination process. The results indicated that by combining wire and powder, the overall deposition rate was increased. While seen in Table 1, sample surface roughness increases as all observed parameters remain constant. Akbari and Kovacevic [14] investigated the mechanical and microstructural properties of 316LSi coupons produced by a robotized laser or wire feed deposition method. In compared to the block samples, the thin-walled samples with slower cooling rates exhibited coarse columnar grains, decreased UTS, and decreased hardness. As shown in Table 1, perpendicular samples exhibited reduced UTS and elongation for both coupon types, indicating weaker bonding at the interlayer or bead interface due to the absence of fusion pores.

Sadhu et al. [51] investigated the influence of cooling rate on fracture mitigation during multilayer DMLD of NiCrSiBC-60 percent WC on Inconel 718. Cracks could not be minimised within the current testing range of 300 mm/min to 700 mm/min by altering the cooling rate or scan speed. As with hardness, the coating's wear resistance rose as the scan speed and substrate preheating temperature were reduced. Yu et al. [50] investigated the cracking behaviour, microstructure, and mechanical properties of austenitic stainless steel components manufactured using LMD using the best process parameters and feedstock powder mixture. The microstructure is composed of fine columnar dendrites that coarsen with height along the building direction. As illustrated in Table 1, this results in a decrease in hardness. The influence of operation settings on the friction and wear of DMD components was examined by Naiju and Anil [44]. The deposit was made of H13 tool steel on a mild steel base. The observations were then analysed, and ANOVA calculations were utilised to ascertain the primary component causing wear. According to general law, the coefficient of friction decreases as the load increases. As shown in Table 1, porosity was also discovered at multiple locations along the wear track due to the microstructure.

Soodi et al. [43] looked into the microstructure and hardness of products made with laser-assisted DMD technology. 316L stainless steel, 420 stainless steel, Stellite(R) 6, tool steel (H13), Chalmoloy (Ni-based alloy), and Aluminium Bronze were among the alloy powders studied. Welded item microstructure and hardness values were compared to those provided in Society of Automotive Engineers (SAE) specifications (as annealed). Laser deposited samples have significantly different hardness and defect characteristics than worked samples, as shown in Table 1. Lewis and Schlienger [55] proved the feasibility of depositing any metal and several intermetallics into near-net form pieces in a single

processing phase utilising DLF and LENS process methods. The pieces are deposited with an arithmetic Ra of 10 m, necessitating an additional finishing step for certain applications to achieve high precision and a polished surface texture, as shown in Table 1. Singh et al. [53] proposed an alternate approach based on LMD of Al 7050 alloy powder coated with nickel. As illustrated in Table 1, the microstructural examination of the deposits revealed that they are free of significant faults such as porosity and lack of fusion. Tensile testing revealed that the friction stir processed (FSP) samples exhibited a strong combination of yield strength (178 MPa), UTS (302 MPa), and elongation (6%). Microstructural examination revealed a systematic change from columnar to equiaxed dendrites from the bottom to the top of each deposited layer.

Wang et al. [22] conducted a series of studies to improve the forming efficiency and quality of parts with unequal widths fabricated using LDMD technology. To construct single tracks with different widths, a novel technique based on a fluctuating laser beam was developed. As shown in Table 1, the top surface unevenness of thin-walled products can be automatically corrected within the -2.5 mm to -5 mm and 0.5 mm to 2.5 mm laser defocusing ranges. Wang et al. [27] investigated the effects of energy distribution on the properties of a series of AISI 316L stainless steel thin-walled parts made effectively by LMD using a variety of pulse laser parameters. The results indicate that the mode of the laser (pulse or continuous wave) and the pulse laser parameters have a substantial effect on the properties of LMD parts. The maximum hardness is indicated in item by a  $T_{\text{pulse}}$  of 10 ms and a  $T_{\text{pause}}$  of 10 ms, and the minimum hardness is indicated in part fabricated by CWL, where the residual stress on z-component exhibits tensile stress at the edge and compressive stress in the central region, but the residual stress on y-component exhibits the opposite trend, as illustrated in Table 1. Bhattacharya et al. [53] investigated the microstructure of AISI 4340 steel that was laser deposited on a rolled mild steel substrate using the DMD process. The microstructure was composed of ferrite, martensite, and cementite phases. The degree of tempering of the martensite phase increases in the same direction as the decrease in microhardness values from the top to the alloy layer, as shown in Table 1.

Dinda et al. [63] exhibited samples of Inconel 625, a nickel-based superalloy synthesised via DMD. It was determined that the microstructure was columnar dendritic and grew epitaxially from the substrate. As demonstrated in Table 1, none of the samples produced in this experiment had significant faults such as cracks, bonding problems, or porosity, demonstrating that Inconel 625 is a desirable material for laser deposition. The microstructure and characteristics of laser DMD zones before and after heat treatment were investigated by Zhang et al. [65]. The effect of DMD parameters on the rate of deposition and the shape of the formed layer was also studied. The results demonstrate that a laser power of 650 W, a scanning speed of 5.8 mm/sec, a beam diameter of 1 mm, a powder feed rate of 6.45 g/min, and a specific energy of 90-130 J/mm<sup>2</sup> are optimal for high Inconel 718 alloy build-up rate. As shown in Table 1, the microhardness of the laser DMD zone after heat treatment was significantly higher than the microhardness of the treatment as deposited. Imran et al. [72] investigated the mechanical properties of bimetallic structures using samples manufactured from H13 tool steel powder clad on a copper alloy substrate via DMD. As illustrated in Table 1, the bond interfaces of several claddings exhibited porous and crack-free transition zones. When compared to H13 tool steel that had a buffer layer of 41C stainless steel, the bond strength of the directly clad H13 tool steel was greater.

The effect of heat treatment at 550 and 1050°C on the structure and tribological properties of nickel-based metal specimens formed by DLD material when introducing counterface, strength and ductility under static loads, and durability under cyclic bending loads was investigated by Gorunov and Gilmutdinov [73]. Heat treatment has been shown to increase the wear resistance of specimens with significant carbide morphology emission. When heated to 550°C, the alignment structure of 1535-30 alloy specimens increases endurance under cyclic bending loads while maintaining the same wear characteristics, as indicated in Table 1. Chen et al. [74] evaluated the microstructure and mechanical properties of the AISi10Mg alloy utilised in AM, as well as the effect of scanning speed on the manufacturing performance of the specimen. As illustrated in Table 1, as scanning speed is decreased, the microhardness of manufactured components drops but the tensile property increases. Froend et al. [75] devised a wire-based LMD technique for the aluminium alloy 5087 (AlMg4.5MnZr). Preheating has been shown to increase porosity and decrease distortion. As illustrated in Table 1, defect-free layers with adaptable geometrical features can be treated and modified to meet specific process requirements.

Kim and Peng [76] studied the impact of wire feeding direction and location, cladding time, and cladding speed on the quality of the laser cladding layer. The wire feeding direction and position, according to the findings, are crucial for wire laser cladding. If the wire feeding direction and placement are correct, the wire can be dipped into the melt pool and melted by the heat of the molten metal. As demonstrated in Table 1, as cladding speed increases, the hardness of the clad layer and heat affected zone increases. The researchers looked into how the laser pulse settings and powder mass flow rates affected the breaking susceptibility of the final deposited structures. Significant longitudinal tensile stresses were created along the tracks during the deposition process, as shown in Table 1, and their magnitude grew as the duty cycle increased. Zhang and colleagues [77] looked into the connection between microstructure, Vickers hardness, mechanical characteristics, process parameters, and TiC concentration. In this investigation, powder mixtures with three distinct volume percentages of Ti6Al4V and TiC were used as feed material. The hardness of the portion increased from 300 VH to 600 VH along its length. No significant change in hardness was seen for any of the processing settings examined, as indicated in Table 1.

Gu et al. [10] investigated the application of additive manufacturing (AM) to create complex-shaped functional metallic components from metals, alloys, and metal matrix composites (MMCs) for the aerospace, defence, automotive, and biomedical industries. Densification mechanisms of powder materials used in AM are described, including pure metal powder, pre-alloyed powder, and multi-component metals or alloys or MMCs powder. The relationship between material, process, and metallurgical mechanism for laser-based additive manufacture of metallic components was developed in

Table 1. Bhattacharya et al. [78] studied the microstructure evolution and mechanical and corrosion parameters of a Cu-30Ni alloy sample during the DMD process. The Cu-30Ni alloy was successfully deposited on a rolled C71500 plate substrate using the DMD process. Microhardness values for the clad were found to be lower than those for the substrate, but they were very consistent across the clad, as shown in Table 1. Zheng et al. [79] improved their grasp of the fundamental physical principles by examining the glass forming ability (GFA), glass transition, crystallization behaviour, and mechanical properties of a glassy alloy. The LENS technology is used to shape Fe-based Fe-B-Cr-C-Mn-Mo-W-Zr metallic glass (MG) components. The microhardness of LENS-treated Fe-based MG components, as revealed in Table 1, is a high 9.52 GPa.

Janaki Ram et al. [80] investigated the feasibility of using the LENS process, an innovative AM approach, to fabricate CoCrMo implants. Through a series of investigations, the optimal conditions for CoCrMo deposition were found. The findings established that, under ideal conditions, the LENS process can produce deposits that are metallurgically sound. As indicated in Table 1, the hardness of the LENS deposited CoCrMo is equivalent to that of regular CoCrMo wrought material. Li et al. [81] demonstrated a metal fine wire feed AM technology capable of producing thin-wall structures with a height-to-width ratio of up to 40 and a core-forming power of less than 50 W. Thermal resistance was employed to alter the gradient parameters in this investigation, which significantly reduced the step effect associated with conventional AM and resulted in  $R_a$  values of less than 5  $\mu\text{m}$ , comparable to those obtained with selective laser melting (SLM). As demonstrated in Table 1, the Vickers hardness was uniform. Shaikh et al. [82] investigated the surface quality of a fine wire-based laser metal deposition (FW-LMD) technology used to fabricate high precision metal components with enhanced resolution and dimension accuracy. The proposed FW-LMD AM process utilises a fine stainless steel wire with a diameter of 100  $\mu\text{m}$  as the additive material and a pulsed Nd:YAG laser as the heat source. According to Table 1, an optimal lateral overlap of 60-70% results in a  $R_a$  of 8 to 16  $\mu\text{m}$  in all printed directions.

Part output parameters such as surface roughness, waviness, and hardness vary in response to changes in input factors such as laser power, scan speed, and powder flow rate, according to the reviewed literature. Furthermore, the wire feed process produces items with superior surface properties as compared to other processes. Steel and titanium-based alloys are said to offer excellent surface characteristics. This paper identifies a research gap in understanding how process variables affect the surface characteristics of components manufactured from distinct materials. This work addresses a research need by examining the effect of process parameters on the surface quality of parts created by powder, wire, and combination deposition techniques. The purpose of this literature review is to have a better understanding of the relationship between input and output characteristics for the four basic types of alloy materials that are usually utilised in industry. This research may be used to find the ideal process parameters for manufacturing components made of a variety of materials for a variety of industrial applications.

## ROUGHNESS

Figure 11 depicts the effect of various process parameters on the surface roughness of several materials. When the laser power is increased from 0.32 to 3.2 kW, the  $R_a$  ranges from 0.7 to 21.14  $\mu\text{m}$  [15,68]. Increasing the laser power from 0.45 kW to 1.5 kW results in a  $R_a$  range of 9.85 to 78  $\mu\text{m}$  for Inconel 718 [16,55]. If the laser power is increased from 0.05 to 1.5 kW, the resulting  $R_a$  is between 0.73 to 158  $\mu\text{m}$  [28,69,81]. Similarly, when the laser power is varied between 0.0435 kW and 0.0514 kW for SS 304, the resulting  $R_a$  is between 8 and 16  $\mu\text{m}$  [82].

We can predict that increasing the Ti6Al4V scanning speed from 0.1 to 3 m/min resulted in  $R_a$  values ranging from 0.7 to 21.14  $\mu\text{m}$  [15,68]. Increasing the scanning speed from 0.3 to 1.2 m/min results in a  $R_a$  range for Inconel 718 of 9.85 to 78  $\mu\text{m}$  [16,55]. When the scanning speed of SS 316L is increased from 0.18 to 0.3 m/min, the  $R_a$  value varies between 0.73 and 158  $\mu\text{m}$  [28,69,81]. In contrast, increasing the scanning speed from 0.24 to 0.6 m/min produces a  $R_a$  in the range of 3.2 to 5.8  $\mu\text{m}$  for Fe 313. Meanwhile, adjusting the scanning speed from 0.09 to 0.3 m/min results in a  $R_a$  of between 8 and 16  $\mu\text{m}$  for SS 304 [82].

**Table 1.** Surface characteristics of various materials

S. No.	Material	Scanning speed (m/min)	Wire feeding angle (deg)	Laser pulse frequency (Hz)	Laser spot size (mm)	Powder defocusing distance (mm)	Laser defocusing distance (mm)	Wire delivery rate (g/min)	Wire feed rate (m/min)	Powder + wire delivery rate (g/min)	Powder flow rate (g/min)	Gas flow rate (l/min)	Laser power (kW)	Powder / wire size (μm)	Roughness R <sub>a</sub> (μm)	Waviness W <sub>t</sub> (μm)	Hardness (HV)	Defects observed	Ref.		
Aluminium based alloy materials																					
1	Aluminium bronze	-	-	-	-	-	-	-	-	-	-	-	-	90 - 150	-	-	180	Finer grain size	[43]		
2	Al 7050 on Al 6061 substrate	0.5	-	-	-	-	-	-	-	-	3.3	20	1.05	5 - 50	-	-	153	No major defects but little porosity	[53]		
3	AlSi10Mg	0.48	-	-	1.2	-	-	-	-	-	23.2	9	1.9	44	-	-	101 - 148	Fine ductile dimples	[74]		
		0.6															110 - 150	-			
		0.72															124 - 198	Tiny pores			
4	AA 5087 on AlMg3 substrate	1	35	-	1.6	-	23	-	1 - 10	-	-	10	3.5 - 4.5	1000	0.2	-	-	Adequate fusion, crack & pores occur	[75]		
Steel based alloy materials																					
1	AISI 316L	0.75	-	-	1.2	-	-	-	-	-	2	8.5	0.57	-	-	-	204 ± 10	Micro-pores & micro-cracks	[50]		
		1									2.7		0.75								
1	AISI 316L	6	-	40	-	-	-	-	-	-	4.68	6.67	1	45 - 150	-	-	257	-	[27]		
				20													224				
				13.33													248				
				100													258				
				0													208				
2	H13 tool steel	0.06	-	-	2.5	-	-	-	-	-	14.22	40.2	0.9	53 - 150	-	-	204 - 600 (x)	Free of micro-porosity and cracks	[83]		
		0.18									28.32		1.2				198 - 599 (y)				
											-		-				-			-	212 - 668 (x)
																					233 - 706 (y)
-	-	-	-	-	-	-	-	-	-	-	-	90 - 150	-	-	657	Finer grain size	[43]				

**Table 1.** Surface characteristics of various materials (cont.)

S. No.	Material	Scanning speed (m/min)	Wire feeding angle (deg)	Laser pulse frequency (Hz)	Laser spot size (mm)	Powder defocusing distance (mm)	Laser defocusing distance (mm)	Wire delivery rate (g/min)	Wire feed rate (m/min)	Powder + wire delivery rate (g/min)	Powder flow rate (g/min)	Gas flow rate (l/min)	Laser power (kW)	Powder / wire size (µm)	Roughness Ra (µm)	Waviness Wt (µm)	Hardness (HV)	Defects observed	Ref.					
3	316L on EN43A substrate	0.24	20	-	-	-	-	-	1.59	-	-	19	1.1	800	17.9	-	-	No porosity	[69]					
			30												20									
			40												60									
			50												30									
			-	0	1.7	-	-	-	-	-	-	8.4	5	0.45	54 - 150	-	-	70	143	Porosity	[28]			
				8.3														60	133	-				
				12.5														58	150	Fluctuating melt pool				
				25														44	151	No voids or cracks				
				50														60	166	unmelted particles				
				100														57	169	-				
				-	1.5	-	-	-	-	-	-	-	3	1.5	53 - 150	-	-	-	No porosity	[70]				
				-	2.88														-		High porosity			
		-		2.88	-														Minimal porosity					
		20		-	1.5	-	-	-	-	-	-	-	-	-	-	-	-	-	-	-	-	-	[70]	
		3																						37.5
		8.4																						39
		11.4	40																					
		14.4	41																					
		3	33.5																					
		8.4	34.8																					
		11.4	36																					
		14.4	38																					
		0.18 - 0.24	-	-	-	-	-	-	-	-	-	-	-	-	-	-	-	-	-	-	-	[13]		
																							7.2	18.6
																							15	24
																							22.5	23.9
																							29.4	35
																							36.6	37
45	45.8																							
7.2	15																							
15	24.9																							
22.5	24.3																							
29.4	22																							
36.6	27																							
45	36.2																							

**Table 1.** Surface characteristics of various materials (cont.)

S. No.	Material	Scanning speed (m/min)	Wire feeding angle (deg)	Laser pulse frequency (Hz)	Laser spot size (mm)	Powder defocusing distance (mm)	Laser defocusing distance (mm)	Wire delivery rate (g/min)	Wire feed rate (m/min)	Powder + wire delivery rate (g/min)	Powder flow rate (g/min)	Gas flow rate (l/min)	Laser power (kW)	Powder / wire size (µm)	Roughness Ra (µm)	Waviness Wt (µm)	Hardness (HV)	Defects observed	Ref.				
		0.18 - 0.24	-	-	-	-	-	-	-	-	-	4.02 - 6	1	53 - 150	17.5	-	-	-					
															19.8								
															35								
															25.7								
															38								
															46								
			32	-	-	-	-	-	-	-	-	-	-	-	4.98 - 15					1.5	800	14	
																						20	
																						24	
																						9	
																						15.5	
																						9.1	
																				1.3	800	23.8	
																						25.6	
		4.5																					
		1																				800	5.5
																				14			
																				15			
																				11			
		-																		-	-	-	-
			21																				
			40																				
			42																				
			21																				
			1.3	53 - 150	20																		
					74																		
					55																		
					27.5																		
1	53 - 150		37																				
		52.8																					
		13.5																					
		20.4																					
-	-	-	-	-	-	-	-	-	-	-	-	-	-	-	21.6								
															27.6								
															28.5								
															12.9								
															13.5								
															1.3	53 - 150	19.8						
																	27.6						
																	10.8						
																	19.08						
															1	53 - 150	25.8						
25.8																							

**Table 1.** Surface characteristics of various materials (cont.)

S. No.	Material	Scanning speed (m/min)	Wire feeding angle (deg)	Laser pulse frequency (Hz)	Laser spot size (mm)	Powder defocusing distance (mm)	Laser defocusing distance (mm)	Wire delivery rate (g/min)	Wire feed rate (m/min)	Powder + wire delivery rate (g/min)	Powder flow rate (g/min)	Gas flow rate (l/min)	Laser power (kW)	Powder / wire size (µm)	Roughness Ra (µm)	Waviness Wt (µm)	Hardness (HV)	Defects observed	Ref.		
4	SS 316L	0.36	-	-	48	-1	-	-	-	-	7.8	8	1	15 - 45	-	-	325	-	-	[18]	
						0											1098				
						1											2866				
						-											2403				
						-											1098				
		0.36	-	-	48	-	3	-	-	-	-	7.8	8	1	15 - 45	-	702	-	-		
		0.45	-	-	5	-	-	-	-	-	-	12	-	0.6	-	-	-	-	-	Homogeneous, Defect-free	[71]
		0.3																	211		
		0.375																	200		
		0.45																	196		
0.3	197																				
0.375	188																				
0.45	180																				
0.3	30 - 60	-																	0.08		
0.3	-	-	0.08	-	-	-	-	-	-	-	-	-	0.05	300	2.3 (y)	-	180				
															1.9 (x)	-	180				
															3.63 (y)	-	180				
5	Fe 313 on SS 304 substrate	0.24	-	-	OD = 3.8, ID = 2.6	-	-	-	-	-	8	-	2	75 - 106	5.8	26	-	-	[19]		
		0.36													3.55	24.5					
		0.48													3.2	18					
		0.6													3.45	14					
		0.84	-	-	1	-	-5	-	-	-	-	8	-	0.6	45 - 74	-	-	-	No pores and micro-cracks	[22]	
6	Fe 313 on 45# steel substrate	0.24	-	-	-	-	-	-	-	-	9	2.5	5	37 - 50	-	-	-	610	Irregular structure	[21]	
																		620			
																		618			Regular structure
																		608			Irregular structure
																		600			
7	316LSi on 304L substrate	0.48	-	-	1.6	-	-10	-	0.72	-	-	15	1	1200	-	-	216	Low porosity	[14]		



**Table 1.** Surface characteristics of various materials (cont.)

S. No.	Material	Scanning speed (m/min)	Wire feeding angle (deg)	Laser pulse frequency (Hz)	Laser spot size (mm)	Powder defocusing distance (mm)	Laser defocusing distance (mm)	Wire delivery rate (g/min)	Wire feed rate (m/min)	Powder + wire delivery rate (g/min)	Powder flow rate (g/min)	Gas flow rate (l/min)	Laser power (kW)	Powder / wire size (µm)	Roughness Ra (µm)	Waviness Wt (µm)	Hardness (HV)	Defects observed	Ref.				
Titanium based alloy materials																							
1	Ti6Al4V	0.3	-	-	2	-	-	-	-	-	2	2	-	-	0.8	13.3	-	-	-	[36]			
															1.2	6.6							
															1.6	5.6							
															2	4.5							
															2.4	2.5							
															2.8	1							
															3.2	0.7							
		0.4	-	-	1.3	-	-	-	-	-	-	-	3	-	0.4	45 - 75	4.9	144	-	-	-	[68]	
																	5.2	130					
																	4.3	148					
		0.1	-	-	1.3	-	-	-	-	-	-	-	3	-	-	45 - 75	0.32	3.5	496	-	-	-	[37]
																	0.4	3	412				
																	0.5	2.8	327				
																	0.32	5	258				
																	0.4	2.5	200				
																	0.5	1.9	189				
																	0.32	4.6	-				
		0.2	-	-	1.3	-	-	-	-	-	-	-	-	-	-	45 - 75	0.4	2.8	153	-	-	-	[31]
																	0.5	2.7	108				
																	0.32	4.6	-				
		0.4	-	-	1.3	-	-	-	-	-	-	-	2	-	-	75	0.32	497	-	-	-	[37]	
																	0.4	431					
																	0.5	408					
																	0.32	251					
0.4	188																						
0.5	206																						
0.32	131																-	Smaller melt pool					
0.1	-	-	1.3	-	-	-	-	-	-	-	2	-	-	75	0.4	111	-	-	-	[37]			
															0.5	103							
															0.32	103							
0.36	-	-	-	-	-	-	-	-	-	-	1.2 – 1.6	16 - 20	1	73 - 108	-	-	-	-	-	Adequate fusion	[31]		



**Table 1.** Surface characteristics of various materials (cont.)

S. No.	Material	Scanning speed (m/min)	Wire feeding angle (deg)	Laser pulse frequency (Hz)	Laser spot size (mm)	Powder defocusing distance (mm)	Laser defocusing distance (mm)	Wire delivery rate (g/min)	Wire feed rate (m/min)	Powder + wire delivery rate (g/min)	Powder flow rate (g/min)	Gas flow rate (l/min)	Laser power (kW)	Powder / wire size (µm)	Roughness Ra (µm)	Waviness Wt (µm)	Hardness (HV)	Defects observed	Ref.
	Inconel 625	0.3	-	-	0.5	-	-	-	-	-	8	-	0.6	45 - 135	-	-	255	No relevant defects such as cracks, bonding error at the interface between deposit and substrate or pores in the deposits	[63]
											10		0.75				254		
											12		0.9				248		
		10									0.6		257						
		12									0.75		260						
		8									0.9		254						
		12									0.6		263						
		8									0.75		262						
		10									0.9		260						
		2									Inconel 718 on SS substrate		1.0-1.4				-		
3	NiCrSiBC-60%WC on Inconel 718 substrate	0.3	-	-	1.6	-	-	-	-	-	10.8	20	0.6	45 - 106	-	-	998	Multiple cracks were formed	[51]
		0.5															976		
		0.7															971		
4	Colmonoy	-	-	-	-	-	-	-	-	-	-	-	-	88 - 152	-	-	376	Granular size	[43]
5	Inconel 690	0.75-0.77	-	-	-	-	-	-	-	-	7-11	-	0.14-0.18	-	10-14	-	-	-	[36]
6	Hoganas (1535-30)	0.7-1.1	-	-	1.3-1.7	-	-	-	-	-	10-14	-	0.7-0.9	43 - 127	-	-	712-714	-	[73]
7	Hoganas (1560-00)	0.5 - 1	-	-	1.3-1.7	-	-	-	-	-	6 - 16	-	0.3 - 1.1	44 - 126	-	-	1120-1124	-	
8	Inconel 600	0.09	-	20	2.5	-	-	-	5.58	-	-	-	0.22	200	-	-	160 - 214	No cracking	[76]
		0.12															169 - 215		
		0.15															184 - 229		
9	Inconel 718	0.4000-0.4500	-	-	1	-	-	-	-	-	6.40-6.50	-	0.60-0.70	48 - 152	-	-	277 - 321	-	[65]

**Table 1.** Surface characteristics of various materials (cont.)

S. No.	Material	Scanning speed (m/min)	Wire feeding angle (deg)	Laser pulse frequency (Hz)	Laser spot size (mm)	Powder defocusing distance (mm)	Laser defocusing distance (mm)	Wire delivery rate (g/min)	Wire feed rate (m/min)	Powder + wire delivery rate (g/min)	Powder flow rate (g/min)	Gas flow rate (l/min)	Laser power (kW)	Powder / wire size (µm)	Roughness Ra (µm)	Waviness Wt (µm)	Hardness (HV)	Defects observed	Ref.	
10	Inconel 718 on Ti6Al4V substrate	0.1-0.5	-	-	1.50-1.65	-	-	-	-	-	10.74	4.00-4.05	0.4-0.8	53 - 150	78	-	-	-	-	
											21.48				62					
											32.22				53					
											10.74				48					
											21.48				46					
											32.22				40					
				10.74	4.00-4.05						1.3-1.7	54								
				21.48								42								
				32.22								31								
				10.74								39								
				21.48								35								
				32.22								25								
11	Inconel 718 + SS 316L on SS 316L substrate	-	-	-	2.3-2.7	-	-	-	-	-	40.40-40.60	-	48 - 152	-	-	-	-	125 - 179	[85]	
																		0.45		127 - 163
																		0.55		131 - 147
																		0.65		128 - 145
																		0.75		135 - 186
																		0.45		136 - 181
																		0.55		127 - 152
																		0.65		129 - 148
																		0.75		
																		48-50		
12	Ni-Co	-	-	-	-	-	-	-	-	-	-	-	3-7	38 - 102	-	-	5	-	[10]	
Other alloy based materials																				
1	Cu-30Ni on C71500 substrate	0.7	-	-	2	-	-	-	-	-	12	-	2	60 - 120	-	-	115 - 130	No cracks but less than 2% porosity	[78]	
2	ASTM F1537 CoCrMo	0.762	-	-	-	-	-	-	-	-	0.57	-	0.285	44	-	-	382	Good bonding without any defects	[80]	
3	Stellite 6	-	-	-	-	-	-	-	-	-	-	-	-	90 - 150	-	-	504	Finer grain size	[43]	

**Table 1.** Surface characteristics of various materials (cont.)

S. No.	Material	Scanning speed (m/min)	Wire feeding angle (deg)	Laser pulse frequency (Hz)	Laser spot size (mm)	Powder defocusing distance (mm)	Laser defocusing distance (mm)	Wire delivery rate (g/min)	Wire feed rate (m/min)	Powder + wire delivery rate (g/min)	Powder flow rate (g/min)	Gas flow rate (l/min)	Laser power (kW)	Powder / wire size (µm)	Roughness Ra (µm)	Waviness Wt (µm)	Hardness (HV)	Defects observed	Ref.
4	Cu on Ti6Al4V substrate	0.3	-	-	4	-	-	-	-	-	-	2	1.2	100 - 200	6.7	-	-	Lateral cracks	[34]
		0.5													3.52			-	
		0.9													1.77			-	
		1.2													1.41			-	
5	W-25Re	0.762	-	-	-	-	-	-	-	-	9	-	0.16	-	-	-	Absence of fusion & porosity are present	[55]	

For Ti6Al4V, we can predict that varying the powder flow rate between 2 and 5.76 g/min results in a  $R_a$  ranging from 0.7 to 21.14  $\mu\text{m}$  [15,68]. Similarly, varying the powder flow rate between 2.5 and 32.22 g/min yields  $R_a$  values ranging from 9.85 to 78  $\mu\text{m}$  [16]. When the powder flow rate is changed from 3.672 to 45 g/min in the instance of 316L, the resulting  $R_a$  ranges from 15 to 70  $\mu\text{m}$  [13,28,70]. The  $R_a$  of Ti6Al4V fluctuates between 0.7 and 21.14  $\mu\text{m}$  when the gas flow rate is changed between 2 and 4 l/min [15]. Similarly, increasing the gas flow rate from 4.02 to 8.04 l/min results in  $R_a$  values ranging between 25 and 78  $\mu\text{m}$ . When the gas flow rate is modulated between 3 and 19 l/min, the resulting  $R_a$  value varies between 4.5 and 158  $\mu\text{m}$  [13,28,69,70].

We may extrapolate that adjusting the laser pulse frequency from 0 to 100 Hz resulted in a  $R_a$  of 44 to 70  $\mu\text{m}$  for SS 316L [28]. In terms of material feeding angle, we can determine that altering the angle between 20 and 60 degrees results in a  $R_a$  of between 0.73 and 158  $\mu\text{m}$  [13,69,70,81]. Similarly, by adjusting the material delivery rate between 0.42 and 9.6 g/min, the  $R_a$  in this material can be varied between 4.5 and 41  $\mu\text{m}$  [13,70]. Additionally, when the wire feed rate is varied between 0.3 and 15.6 m/min, the resulting  $R_a$  varies between 0.73 and 74  $\mu\text{m}$  [13,69,81].

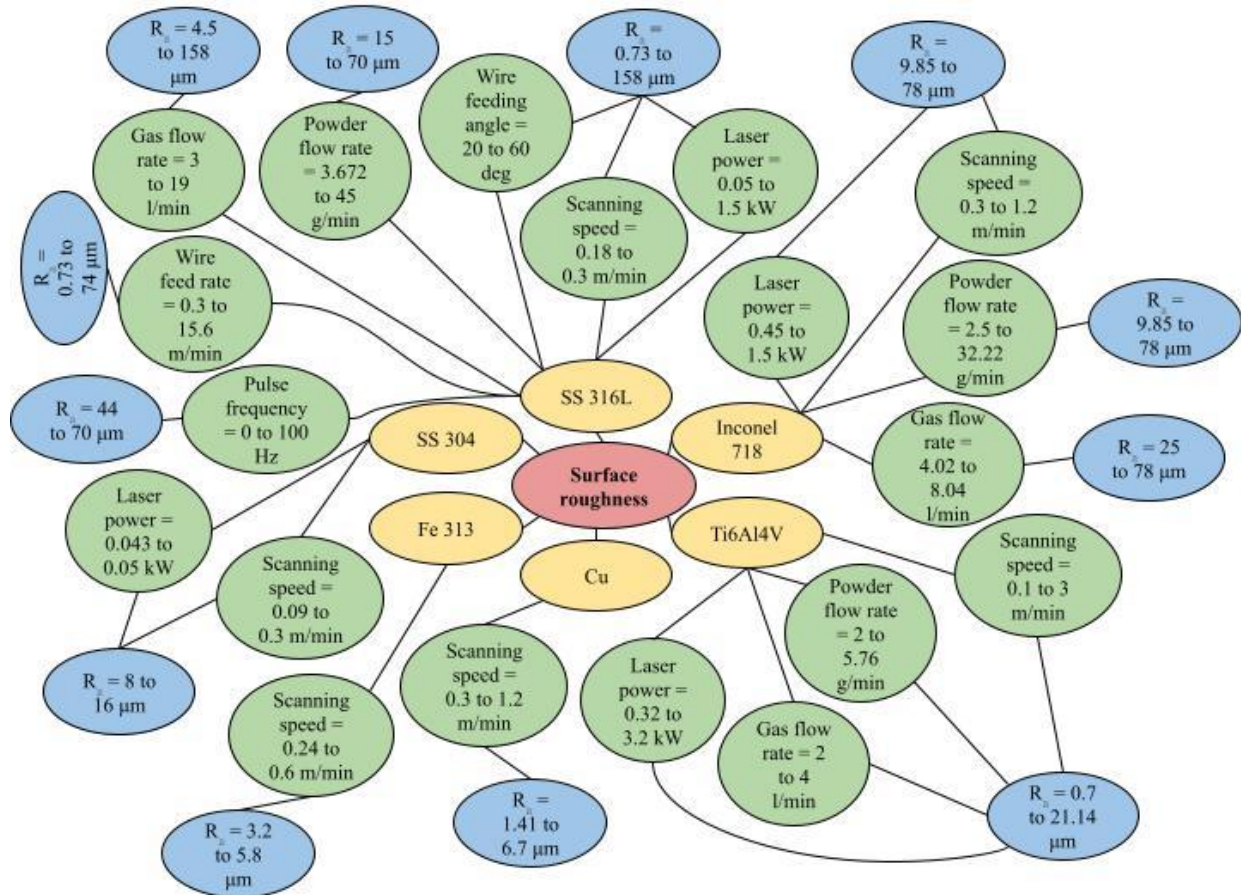


Figure 11. Effect of surface roughness on various materials

## Topography

When Ti-15Mo is deposited vertically, the surface roughness is larger than when it is deposited horizontally. As a result, the surface topography of vertically deposited samples is poor [46]. Surface roughness is lower in titanium-based alloys, such as Ti6Al4V, than in other materials-based alloys. As a result, it appears that the surface topography of these alloys has improved. Similarly, at high process parameter levels, surface roughness is reduced for steel-based alloys. As a result, we can obtain a more precise picture of the surface topography. Poor topography would result if surface roughness was high at low values of process parameters such as laser power, feeding angle, and so on.

## Texture

The surface texture of copper-based alloys improves significantly with increasing laser power [34]. The surface of the top layer of nickel-based alloy materials is rougher than the rest of the product. As a result, the surface texture of the top layer is rough [16]. Similarly, for steel-based alloy materials, the surface roughness is increased as a result of lower process parameter values, and a smooth and clear surface texture is not attained. Additional polishing operations, on the other hand, are necessary to obtain a smooth surface texture.

## WAVINESS

The influence of various process parameters on the surface waviness of many materials is depicted in Figure 12. It can be extrapolated that varying the laser power between 0.32 kW and 0.5 kW resulted in a Ti6Al4V  $W_t$  ranging from 103 to 497  $\mu\text{m}$ . Similarly, increasing the powder flow rate from 2 to 3 g/min leads in  $W_t$  values in this material ranging from 103 to 497  $\mu\text{m}$ . Furthermore, increasing the scanning speed from 0.1 to 0.4 m/min yields a  $W_t$  range from 103 to 497  $\mu\text{m}$  [37,68]. Similarly, changing the scanning speed from 0.24 to 0.6 m/min leads in a range of  $W_t$  values between 14 and 26  $\mu\text{m}$  for Fe 313 [19].

We may deduce that altering the particle defocusing distance from -1 to 1 mm resulted in a  $W_t$  of 325 to 2866  $\mu\text{m}$  for SS 316L. Similarly, by adjusting the defocusing distance of the laser from -3 to 3 mm, the resulting  $W_t$  in this material varies between 702 and 2403  $\mu\text{m}$ .

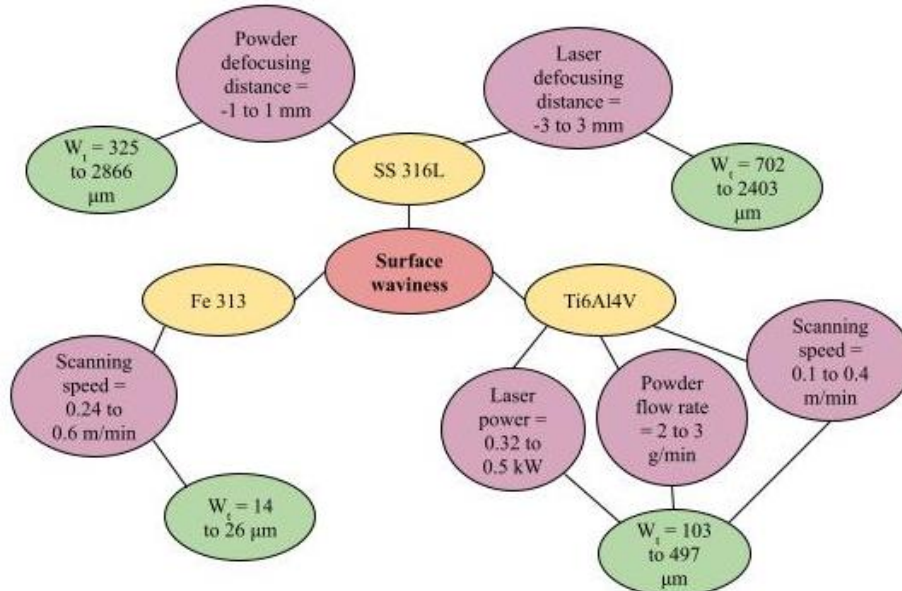


Figure 12. Effect of waviness on various materials

## HARDNESS

The influence of various process parameters on the surface hardness of many materials is depicted in Figure 13. We may estimate that increasing the laser power from 0.4 to 0.7 kW leads in surface hardness (Vickers hardness) values ranging from 304 to 631 HV. Increasing the laser power from 0.6 kW to 0.9 kW results in an Inconel 625 hardness range of 248 to 262 HV [63]. When the laser power is increased from 0.45 to 0.75 kW and Inconel 718 and SS 316L are combined, the hardness ranges between 125 and 186 HV. Similarly, increasing the laser power from 0.5 to 1 kW results in a hardness range of 133 to 258 HV for SS 316L [27,28,50]. When the laser power is varied between 0.9 and 1.2 kW, the resultant hardness of H13 tool steel varies between 198 and 706 HV [49]. Similarly, SS 304 hardness values range from 164 to 243 HV when the laser power is varied between 0.046 and 0.75 kW [50,82].

When the scanning speed is increased from 0.2 to 0.4 m/min, the resulting Vickers hardness for the combination of Ti6Al4V and TiC material is in the range of 304 to 631 HV. Similarly, increasing the Inconel 625 scanning speed from 0.3 to 0.45 m/min results in a hardness of 248 to 262 HV [63]. When the scanning speed is increased from 0.3 to 0.7 m/min, the hardness of NiCrSiBC-60 percent WC ranges from 971 to 998 HV [51]. In example, altering the scanning speed between 0.24 and 6 m/min results in a hardness range of 133 to 258 HV for SS 316L [27,28,50]. When the scanning speed of H13 tool steel is varied from 0.06 to 0.18 m/min, the resulting hardness varies between 198 and 706 HV [49]. Similarly, SS 304 hardness values range from 164 to 243 HV when scanning at 0.18 to 1 m/min [50,82]. When the scanning speed of Inconel 600 is increased from 0.09 to 0.15 m/min, the resultant hardness ranges from 160 to 229 HV [76]. When the scanning speed is adjusted between 0.508 and 1.014 m/min, the hardness of Fe-B-Cr-C-Mn-Mo-W-Zr varies between 678 and 1048 HV [79]. When the scanning speed of AlSi10Mg is increased from 0.48 to 0.72 m/min, the resultant hardness ranges between 101 and 198 HV [74].

The powder flow rate is varied from 2.88 to 5.76 g/min, resulting in a Vickers hardness of 318.5 to 345 HV for Ti6Al4V. Similarly, adjusting the powder flow rate between 8 and 12 g/min results in a hardness range of 248 to 262 HV for Inconel 625 [63]. The hardness of Inconel 718 and SS 316L powders ranges between 125 and 186 HV when the flow rate is raised from 40.44 to 49.92 g/min. In example, when the powder flow rate of SS 316L is varied between 2 and 12 g/min, the resulting hardness ranges between 133 and 258 HV [27,28,50]. When the powder flow rate of H13 tool steel is varied between 14.22 and 28.32 g/min, the resulting hardness varies between 198 and 706 HV [49].

When the pulse frequency is varied between 0 and 100 Hz, the resulting hardness for SS 316L is between 133 and 258 HV [27,28,50]. Similarly, changing the pulse frequency between 500 and 830 Hz results in a hardness of 238 to 243

HV for SS 304 [82]. Variation of the gas flow rate from 2 to 4 l/min results in a surface hardness of 318.5 to 345 HV for Ti6Al4V. Similarly, SS 316L has a hardness range of 133 to 258 HV when the gas flow rate is varied between 5 and 8.5 l/min [27,28,50].

We may deduce that changing the particle defocusing distance from -2 to 2 mm results in a hardness range of 600 to 620 HV for Fe 313 [20]. We may determine that altering the material feeding angle between 30 and 60 degrees resulted in a surface hardness of 170 to 180 HV for SS 316L. Additionally, when the wire feed rate is varied between 0.3 and 0.45 m/min, the resulting surface hardness of this material varies between 170 and 180 HV [81].

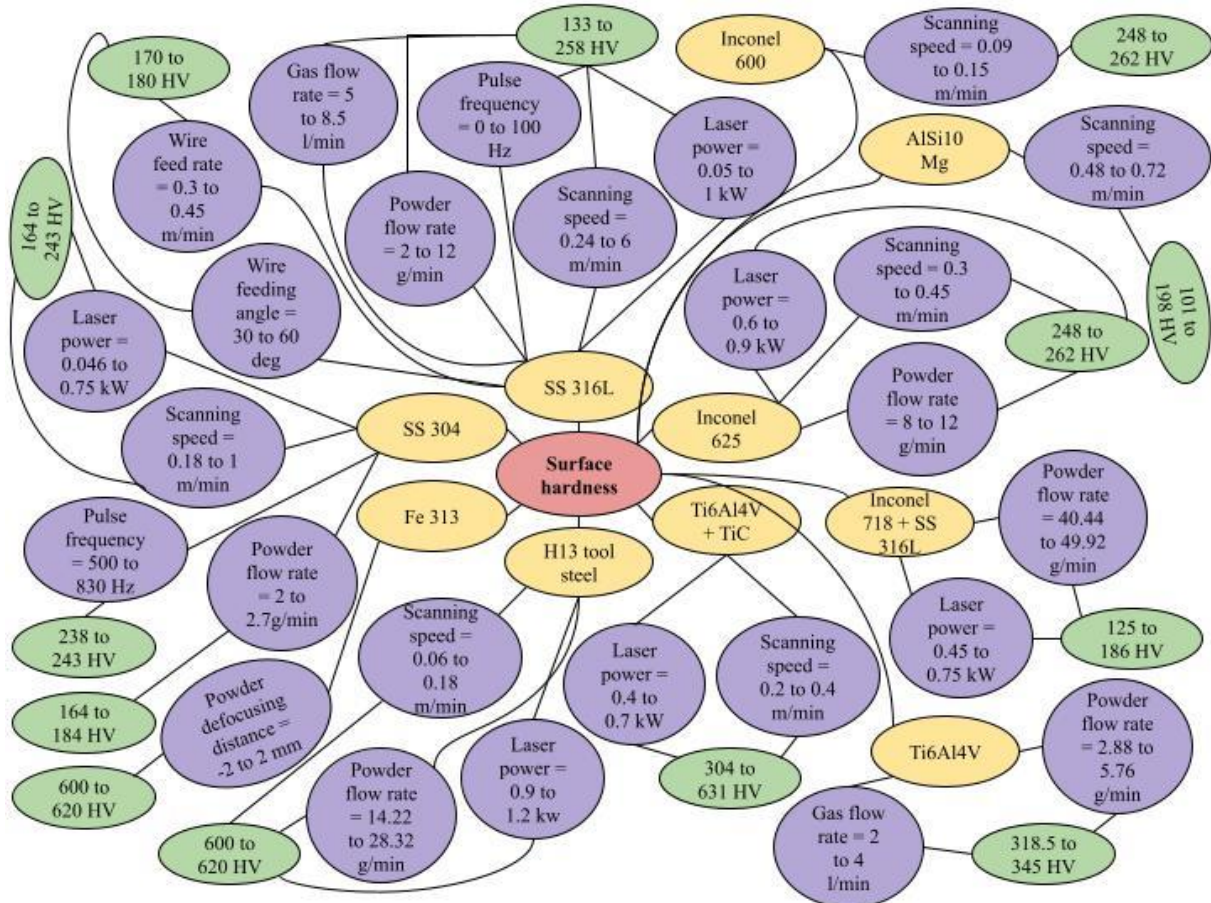


Figure 13. Effect of hardness on various materials

## DEFECTS

The influence of various process parameters on surface defects in various materials is depicted in Figure 14. We can estimate that microcracks formed when the laser power was held between 0.4 and 0.7 kW for the Ti6Al4V and TiC powder material combination. Pores formed in Inconel 625 deposits when the laser power was increased from 0.6 to 0.9 kW [63]. When the laser power was held between 0.45 and 0.75 kW, porosity was reduced in the combination of Inconel 718 and SS 316L powder material. When the laser power was varied between 3.5 and 4.5 kW, cracks and pores formed in the AA5087 metal [75]. In comparison, when the laser power was held between 0.57 and 0.75 kW, no cracking occurred in SS 304 [50].

When the scanning speed is held between 0.3 and 0.7 m/min, many cracks appear on the surface of NiCrSiBC-60 percent WC [51]. Similarly, when the scanning speed was changed between 0.09 and 0.15 m/min, no cracking was seen in Inconel 600 [76]. When the scanning speed was kept between 0.48 and 0.72 m/min in the instance of AlSi10Mg, dimples and small pores developed [74]. In comparison, when the scanning speed was varied between 0.4 and 0.5 m/min, the surface porosity of SS 4340 was low [66]. No surface defects were identified when the scanning speed for SS 304 was varied between 0.09 and 0.3 m/min [82]. Similarly, when the scanning speed was fixed between 0.06 and 0.25 m/min, no surface defects were identified for H13 tool steel [49]. Microcracks and micropores appear in SS 316L when the scanning speed is changed between 0.75 and 1 m/min [50].

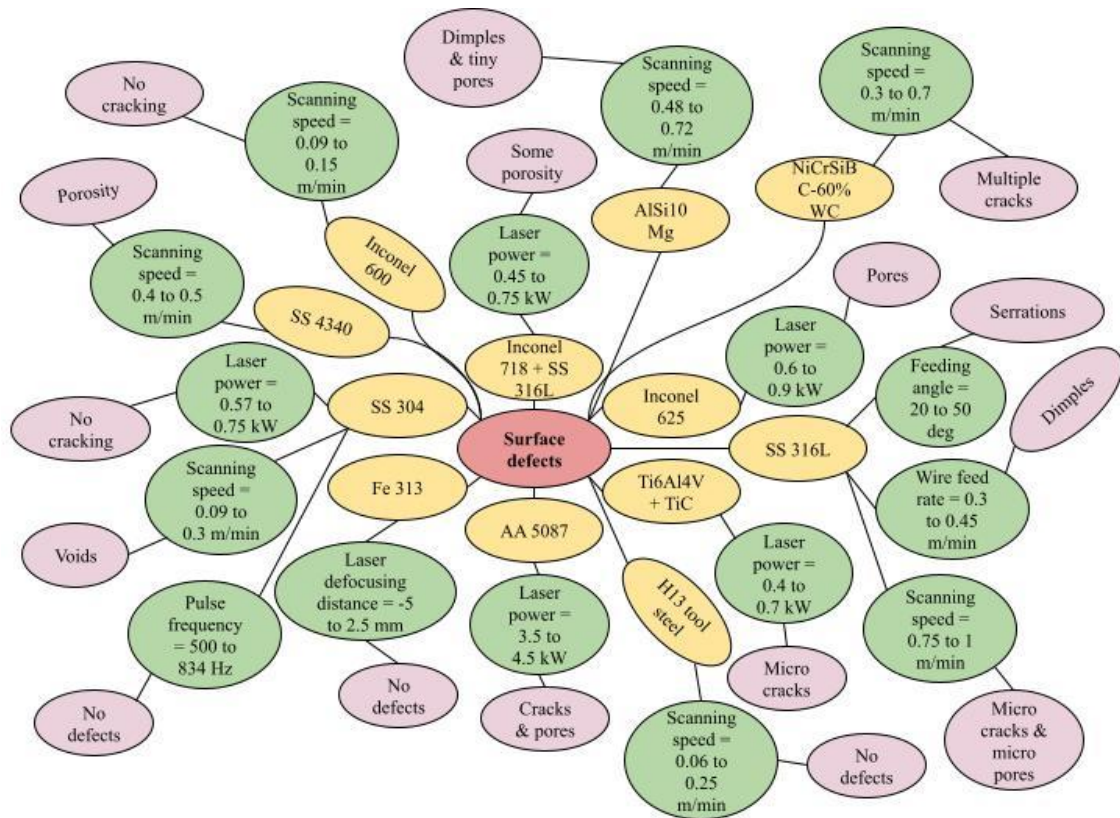


Figure 14. Effect of surface defects on various materials

For SS 304, we can deduce that no surface defects occur when the laser pulse frequency is kept between 500 and 834 Hz [50]. Similarly, when the laser defocusing distance was varied between -5 and 2.5 mm for Fe 313, no defects were seen [22]. In the case of SS 316L, serrations occur when the material feeding angle is changed between 20 and 50 degrees [69]. Similarly, dimples occur on the surface of the stainless steel 316L material when the wire feed rate is maintained between 0.3 and 0.45 m/min [81].

Microstructure

The scanning electron microscopy (SEM) image of copper powder reveals spherical particles with uneven size distribution. The multiple defects and microstructures discovered at various process parameter values are depicted in Figure 15 [34].

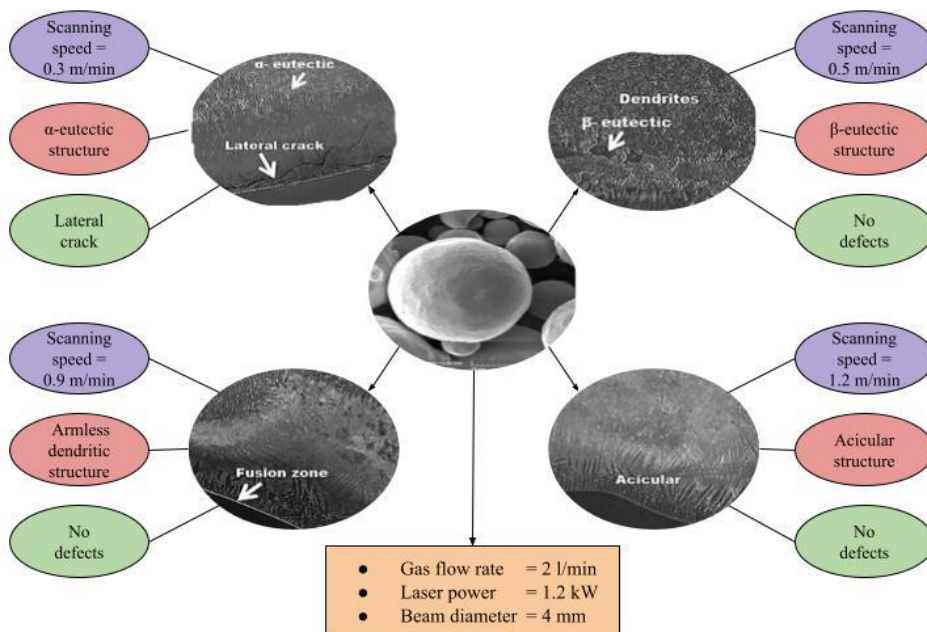
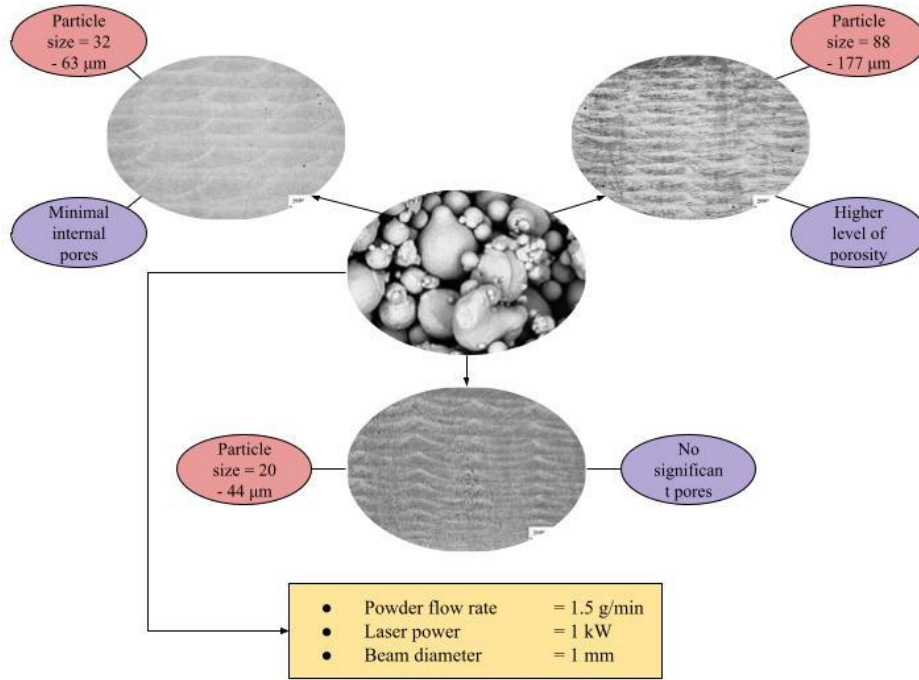


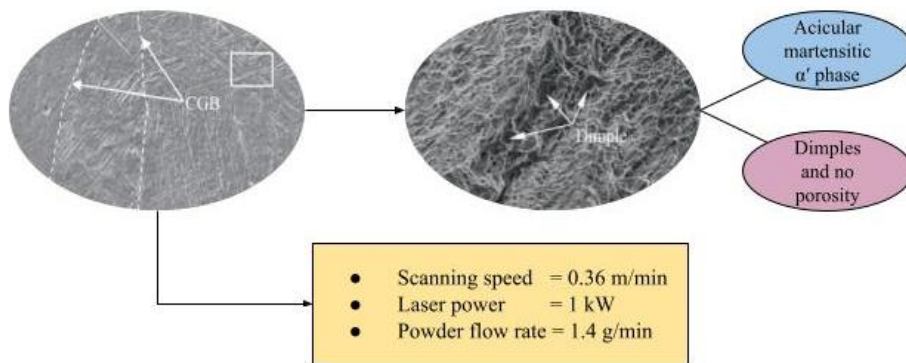
Figure 15. Change in microstructure at different process parameter levels on Cu sample

The SEM image in Figure 16 illustrates the level of porosity identified at various process parameter settings.



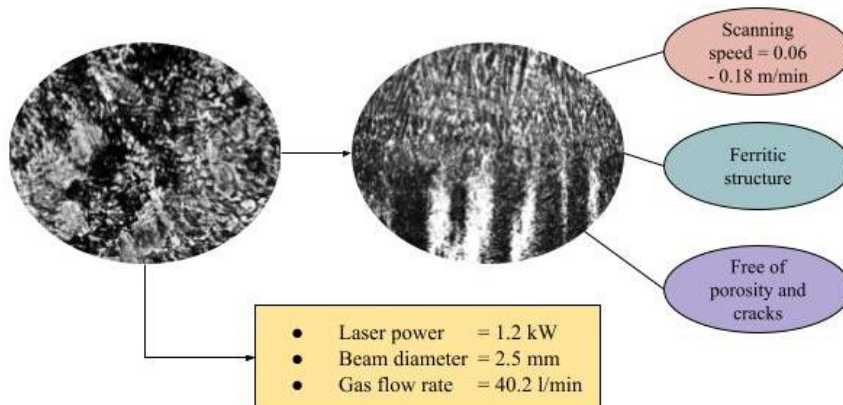
**Figure 16.** Change in microstructure at different process parameter levels on Inconel 625 sample

Figure 17 illustrates the Ti6Al4V sample's deposited microstructure. Numerous observations of continuous grain boundaries (CGB) have been made. The fracture cross-section contracts, and the sample's fracture morphologies exhibit typical dimple fracture toughness characteristics. Shallow dimples cover the fracture surface [31].



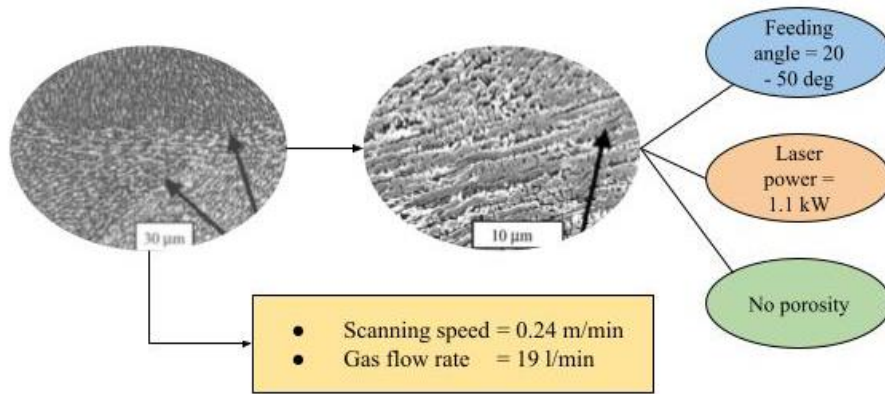
**Figure 17.** Change in microstructure at different process parameter levels on Ti6Al4V sample

Figure 18 shows a higher magnification optical micrograph of the deposition area and fusion zone of a typical H13 steel sample. The microstructure of the restored zone is typically uniform, with no micro-porosity or fissures [49].



**Figure 18.** Change in microstructure at different process parameter levels on H13 steel sample

The multilayer stainless steel 316L material parts adhered well to the tracks. Figure 19 demonstrates that there is no porosity between the layers for wire front feeding [69].



**Figure 19.** Change in microstructure at different process parameter levels on SS 316L sample

The NiCrSiBC-60% WC powder seen in the above backscattered electrons (BSE) photograph is a composite material composed of cast tungsten carbide and self-fluxing NiCrSiBC. A cross-sectional view of materials deposited at varied scan speeds and preheating temperatures is shown in Figure 20. As the cooling rate increased, several fractures appeared at the surface interface [51].

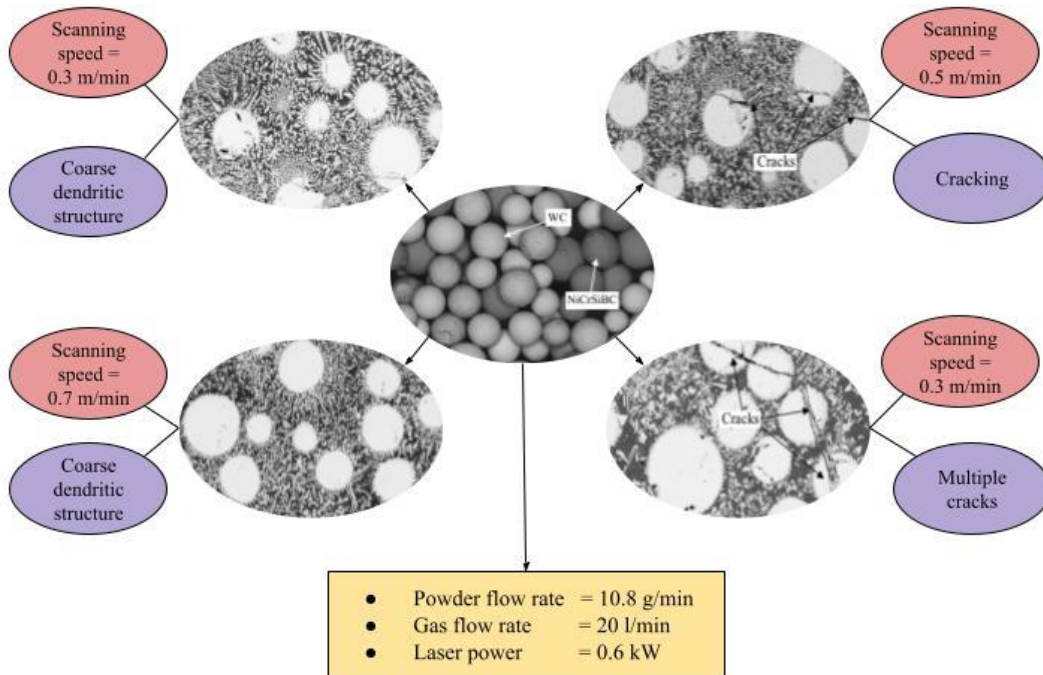


**Figure 20.** Change in microstructure at different process parameter levels on NiCrSiBC-60% WC sample

The shape of Ni-coated Al 7050 powder particles is depicted in Figure 21. It is worth noting that the Ni coating was deposited using physical vapour deposition. The deposition density in the nickel-covered Al 7050 alloy as deposited was greater than 99.5 percent. As illustrated in the SEM image above, no serious faults such as cracks or debonding were observed at the layer contact [53].

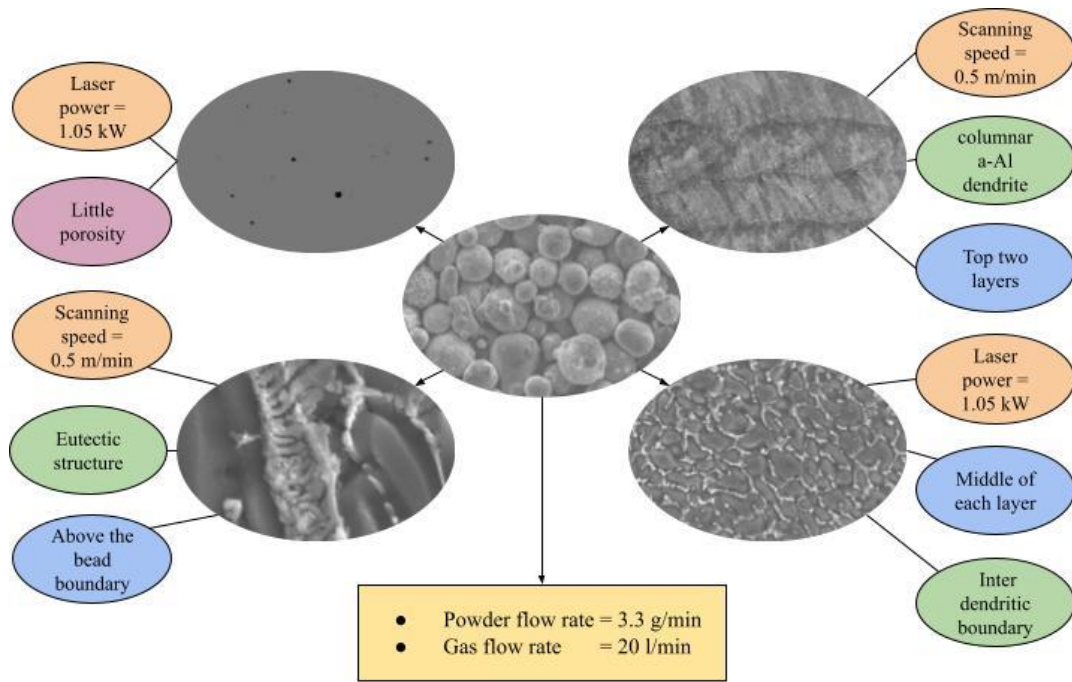


**Figure 21.** Change in microstructure at different process parameter levels on Al 7050 sample

The morphology depicted above is that of powder particles in their natural form. Figure 22 illustrates the flaws caused by varying process parameter values, including variations in porosity, non-bonding at the layer interface, and voids in the deposited samples [66].

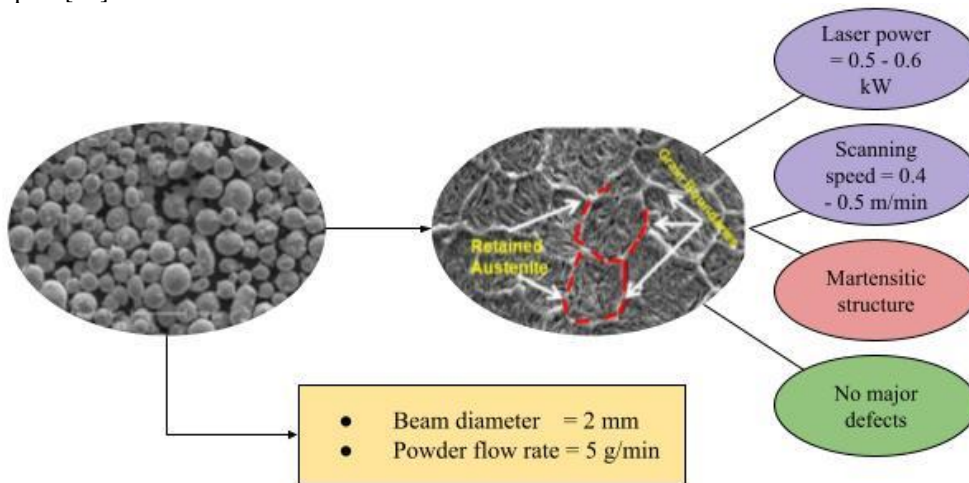


**Figure 22.** Change in microstructure at different process parameter levels on SS 4340 sample

## SUMMARY

In AM material is built up, with each layer comprising a smaller cross-section of a component produced from the initial CAD data. The DMD process allows for the use of many materials at the same time. It makes use of a laser's coherence and directionality to produce a melt pool on the surface of the substrate. DMD technology can be used in the aerospace, automotive, and healthcare industries. This method necessitates the use of a powder feed or wire feed system to feed material into the machine. The qualities of the part are influenced by process variables such as scanning speed, laser power, laser defocusing distance, powder defocusing distance, laser pulse frequency, laser spot diameter, powder stream rate, and gas flow rate. Roughness, finish, texture, waviness, topography, and flaws are surface properties of the component.

As the O<sub>2</sub> component of the shielding gas is lowered during powder feed metal deposition, the roughness of the object reduces while the waviness increases. As the laser power and scanning speed are increased, the waviness value drops. In contrast, identical conditions cause an increase in roughness. As the distance between the laser and the powder grows, the surface waviness and roughness diminish. As a result, increasing the distance between the laser and the powder, as well as the laser power and scanning speed, yields goods with lower surface roughness. When the flow velocity of powder is raised while the laser intensity remains constant, the roughness value increases as well. The hardness of the gas rises with the flow rate. A high value of hardness can be achieved by reducing the rate of powder feed while raising the rate of

gas stream. When the powder particle size is lowered, the three-dimensional surface roughness increases and the number of pores created decreases. The hardness of the part rises as the powder flow rate and scanning speed increase. When a pulsed laser beam is used instead of a continuous laser beam and the powder feed rate is increased, the  $R_a$  of the product drops while the hardness increases.

The hardness of wire feed metal deposition increases as the laser scanning speed increases. Roughness diminishes as the rear feeding arrangement's wire feeding angle increases, and similarly as the front feeding arrangement's wire feeding angle lowers. When deposition happens at the tail end rather than the centre, a more accurate value for the surface roughness is produced. Reduce the pace of wire delivery and the roughness characteristics decrease. When employing a pulsed laser setup with decreasing frequency, the hardness value initially decreases and then increases. To summarise, the  $R_a$  value of wire feed metal deposition is lower than that of powder feed metal deposition. The surface roughness of a powder and wire feed deposition method is the same as that of a powder feed deposition procedure.

## CONCLUSIONS

Surface characteristics are essential to part quality since they determine the component's appearance and part integrity. This study discusses the DMD process component's surface properties for a wide range of materials, the variation of surface qualities as a function of operating conditions has been studied. The best process variables for achieving the best surface attributes can be identified with the help of this study. This research aids in identifying appropriate process parameters for the production of a variety of materials used in a various of applications. The investigation revealed the following crucial findings.

- 1) When compared to metal deposition techniques that use powder feed and mixed deposition, wire feed operations produce surfaces with better surface properties.
- 2) A pulsed laser arrangement out performs wire and powder feed operations as compared to a continuous laser setup.
- 3) Surface roughness is reduced when influencing elements including scanning speed, laser power, feeding angle, and laser frequency are set to high values. Lower surface roughness exhibits better surface finish characteristics with enhanced surface topography.
- 4) When the primary influencing factors, such as scan speed and laser power increases, the surface waviness decreases.
- 5) Porosity and cracking defects are predominant when the process parameters are operated at lower ranges.

## REFERENCES

- [1] I. Gibson, "Rapid prototyping: A review," in *Virtual Modelling and Rapid Manufacturing: Advanced Research in Virtual and Rapid Prototyping*, Leiria, Portugal, 2005.
- [2] S. Pratheesh Kumar, S. Elangovan, R. Mohanraj, and J. R. Ramakrishna, "Review on the evolution and technology of state-of-the-art metal additive manufacturing processes," *Materials Today*, vol. 46, no. 11, 2021.
- [3] I. Gibson, B. Stucker, and D. W. Rosen, *Additive Manufacturing Technologies*. New York, NY: Springer, 2009.
- [4] X. Yan and P. Gu, "A review of rapid prototyping technologies and systems," *Computer-Aided Design*, vol. 28, no. 4, pp. 307–318, 1996.
- [5] R. M. Mahamood, *Laser Metal Deposition Process of Metals, Alloys, and Composite Materials*, 1st ed. Cham, Switzerland: Springer International Publishing, 2017.
- [6] B. de La Batut, O. Fergani, V. Brotan, M. Bambach, and M. El Mansouri, "Analytical and numerical temperature prediction in direct metal deposition of Ti6Al4V," *Journal of Manufacturing and Materials Processing*, vol. 1, no. 1, p. 3, 2017.
- [7] R. M. Mahamood and E. T. Akinlabi, "Experimental analysis of functionally graded materials using laser metal deposition process (case study)," in *Functionally Graded Materials*, Cham: Springer International Publishing, pp. 69–92, 2017.
- [8] A. J. Pinkerton, "Laser direct metal deposition: theory and applications in manufacturing and maintenance," in *Advances in Laser Materials Processing*, Elsevier, pp. 461–491, 2010.
- [9] S. P. Kumar, S. Elangovan, R. Mohanraj, and B. Srihari, "Critical review of off-axial nozzle and coaxial nozzle for powder metal deposition," *Materials Today*, vol. 46, no. 17, pp. 8066–8079, 2021.
- [10] D. D. Gu, W. Meiners, K. Wissenbach, and R. Poprawe, "Laser additive manufacturing of metallic components: Materials, processes and mechanisms," *International Materials Reviews*, vol. 57, no. 3, pp. 133–164, 2012.
- [11] A. Singh, S. Kapil, and M. Das, "A comprehensive review of the methods and mechanisms for powder feedstock handling in directed energy deposition," *Additive Manufacturing*, vol. 35, p. 101388, 2020.
- [12] G. Piscopo, E. Atzeni, and A. Salmi, "A hybrid modeling of the physics-driven evolution of material addition and track generation in laser powder directed Energy Deposition," *Materials (Basel)*, vol. 12, no. 17, p. 2819, 2019.
- [13] W. U. H. Syed, A. J. Pinkerton, and L. Li, "Simultaneous wire- and powder-feed direct metal deposition: An investigation of the process characteristics and comparison with single-feed methods," *Journal of Laser Applications*, vol. 18, no. 1, pp. 65–72, 2006.

- [14] M. Akbari and R. Kovacevic, "An investigation on mechanical and microstructural properties of 316LSi parts fabricated by a robotized laser/wire direct metal deposition system," *Additive Manufacturing*, vol. 23, pp. 487–497, 2018.
- [15] R. M. Mahamood, E. T. Akinlabi, and M. G. Owolabi, "Effect of laser power and powder flow rate on dilution rate and surface finish produced during laser metal deposition of Titanium alloy," presented at the *8th International Conference on Mechanical and Intelligent Manufacturing Technologies (ICMIMT)*, Cape Town, South Africa, 2017.
- [16] S. Dadbakhsh, L. Hao, and C. Y. Kong, "Surface finish improvement of LMD samples using laser polishing," *Virtual and Physical Prototyping*, vol. 5, no. 4, pp. 215–221, 2010.
- [17] S. P. Kumar, R. N. Anthuvan, K. Anand, S. S. Raj, P. M. S. Dhaman, and M. S. Kumar, "Technology overview of metal additive manufacturing processes," *AIP Conference Proceeding*, vol. 2460, p. 040003, 2022.
- [18] G. Zhu, D. Li, A. Zhang, G. Pi, and Y. Tang, "The influence of laser and powder defocusing characteristics on the surface quality in laser direct metal deposition," *Optics & Laser Technology*, vol. 44, no. 2, pp. 349–356, 2012.
- [19] J. Zhang, S. Shi, G. Fu, J. Shi, G. Zhu, and D. Cheng, "Analysis on surface finish of thin-wall parts by laser metal deposition with annular beam," *Optics & Laser Technology*, vol. 119, p. 105605, 2019.
- [20] H. S. Sun, S. H. Shi, G. Y. Fu, J. Zhang, C. Wang, and H. Y. Li, "Effect of defocus distance on layer quality in insider-laser coaxial powder feeding laser cladding," *Advanced Materials Research*, vol. 287–290, pp. 2419–2422, 2011.
- [21] P. Gao, Z. Wang, and X. Zeng, "Effect of process parameters on morphology, sectional characteristics and crack sensitivity of Ti-40Al-9V-0.5Y alloy single tracks produced by selective laser melting," *International Journal of Lightweight Materials and Manufacture*, vol. 2, no. 4, pp. 355–361, 2019.
- [22] L. Wang, G. Zhu, T. Shi, J. Wu, B. Lu, G. Fu and Y. Ye, "Laser direct metal deposition process of thin-walled parts using variable spot by inside-beam powder feeding," *Rapid Prototyping Journal*, vol. 24, no. 1, pp. 18–27, 2018.
- [23] M. F. Erinosh, E. T. Akinlabi, and S. Pityana, "Effect of powder flow rate and gas flow rate on the evolving properties of deposited Ti6Al4V/Cu composites," *Advanced Materials Research*, vol. 1016, pp. 177–182, 2014.
- [24] L. Li, Y. Huang, C. Zou, and W. Tao, "Numerical study on powder stream characteristics of coaxial laser metal deposition nozzle," *Crystals (Basel)*, vol. 11, no. 3, p. 282, 2021.
- [25] W. Li, X. Zhang, and F. Liou, "Modeling analysis of argon gas flow rate's effect on pre-mixed powder separation in laser metal deposition process and experimental validation," *International Journal of Advanced Manufacturing Technology*, vol. 96, no. 9–12, pp. 4321–4331, 2018.
- [26] M. P. Jahan, M. Rahman, and Y. S. Wong, "Micro-electrical discharge machining (micro-EDM)," in *Comprehensive Materials Processing*, Elsevier, pp. 333–371, 2014.
- [27] X. Wang, D. Deng, H. Yi, H. Xu, S. Yang, and H. Zhang, "Influences of pulse laser parameters on properties of AISI316L stainless steel thin-walled part by laser material deposition," *Optics & Laser Technology*, vol. 92, pp. 5–14, 2017.
- [28] A. J. Pinkerton and L. Li, "An investigation of the effect of pulse frequency in laser multiple-layer cladding of stainless steel," *Applied Surface Science*, vol. 208–209, pp. 405–410, 2003.
- [29] S. Pratheesh Kumar, S. Elangovan, R. Mohanraj, and V. Sathya Narayanan, "Significance of continuous wave and pulsed wave laser in direct metal deposition," *Materials Today*, vol. 46, no. 17, pp. 8086–8096, 2021.
- [30] E. Govekar, A. Jeromen, A. Kuznetsov, M. Kotar, and M. Kondo, "Annular laser beam based direct metal deposition," *Procedia CIRP*, vol. 74, pp. 222–227, 2018.
- [31] D. Cheng, J. Zhang, T. Shi, G. Li, J. Shi, L. Lu and G. Fu, "Microstructure and mechanical properties of additive manufactured Ti-6Al-4V components by annular laser metal deposition in a semi-open environment," *Optics & Laser Technology*, vol. 135, p. 106640, 2021.
- [32] K. Kumar, N. Kumari, and J. P. Davim, *Non-Conventional Machining in Modern Manufacturing Systems*. IGI Global, USA, 2019.
- [33] S. A. Lawal and M. B. Ndaliman, "Surface roughness characteristics in finish electro-discharge machining process," in *Encyclopedia of Smart Materials*, Elsevier, pp. 477–487, 2017.
- [34] M. F. Erinosh, E. T. Akinlabi, and O. T. Johnson, "Effect of scanning speed on the surface roughness of laser metal deposited copper on titanium alloy," *Materials Research*, vol. 22, no. 5, pp. 1–6, 2019.
- [35] S. Pratheesh Kumar, S. Elangovan, R. Mohanraj, and J. R. Ramakrishna, "A review on properties of Inconel 625 and Inconel 718 fabricated using direct energy deposition," *Materials Today*, vol. 46, no. 17, pp. 7892–7906, 2021.
- [36] M. Rombouts, G. Maes, W. Hendrix, E. Delarbre, and F. Motmans, "Surface finish after laser metal deposition," *Physics Procedia*, vol. 41, pp. 810–814, 2013.
- [37] M. Gharbi, P. Peyre, C. Gorny, M. Carin, S. Morville, P. Le Masson *et al.*, "Influence of various process conditions on surface finishes induced by the direct metal deposition laser technique on a Ti-6Al-4V alloy," *Journal of Materials Processing Technology*, vol. 213, no. 5, pp. 791–800, 2013.
- [38] M. Alimardani, V. Fallah, M. Irvani-Tabrizipour, and A. Khajepour, "Surface finish in laser solid freeform fabrication of an AISI 303L stainless steel thin wall," *Journal of Materials Processing Technology*, vol. 212, no. 1, pp. 113–119, 2012.
- [39] V. G. Gusev and A. A. Fomin, "Multidimensional model of surface waviness treated by shaping cutter," *Procedia Engineering*, vol. 206, pp. 286–292, 2017.
- [40] M. H. Shojaeefard, A. Khalkhali, and S. Shahbaz, "Analysis and optimization of the surface waviness in the single-point incremental sheet metal forming," *Proceedings of the Institution of Mechanical Engineers, Part E: Journal of Process Mechanical Engineering*, vol. 233, no. 4, pp. 919–925, 2019.

- [41] W. Grzesik, "Surface Integrity," in *Advanced Machining Processes of Metallic Materials*, 2<sup>nd</sup> Edition, Elsevier, 2016.
- [42] H. Shen, C. Liao, J. Zhou, and K. Zhao, "Two-step laser based surface treatments of laser metal deposition manufactured Ti6Al4V components," *Journal of Manufacturing Processes*, vol. 64, pp. 239–252, 2021.
- [43] M. Soodi, M. Brandt, and S. H. Masood, "A study of microstructure and surface hardness of parts fabricated by laser direct metal deposition process," *Advanced Materials Research*, vol. 129–131, pp. 648–651, 2010.
- [44] C. D. Naiju and P. M. Anil, "Influence of operating parameters on the reciprocating sliding wear of direct metal deposition (DMD) components using Taguchi method," *Procedia Engineering*, vol. 174, pp. 1016–1027, 2017.
- [45] Q. Wang, S. Zhang, C. H. Zhang, C. L. Wu, L. Ren *et al.*, "Functionally graded stainless steel fabricated by direct laser deposition: Anisotropy of mechanical properties and hardness," *Acta Metallurgica Sinica (English Letters)*, vol. 31, no. 1, pp. 19–26, 2018.
- [46] T. Bhardwaj, M. Shukla, N. K. Prasad, C. P. Paul, and K. S. Bindra, "Direct laser deposition-additive manufacturing of ti–15Mo alloy: Effect of build orientation induced surface topography on corrosion and bioactivity," *Metals and Materials International*, vol. 26, no. 7, pp. 1015–1029, 2020.
- [47] L. Cao, S. Chen, M. Wei, Q. Guo, J. Liang, C. Liu, M. Wang, "Study of surface topography detection and analysis methods of direct laser deposition 24CrNiMo alloy steel," *Optics & Laser Technology*, vol. 135, p. 106661, 2021.
- [48] Y. Wu, B. Cui, and Y. Xiao, "Crack detection during laser metal deposition by infrared monochrome pyrometer," *Materials (Basel)*, vol. 13, no. 24, p. 5643, 2020.
- [49] W. Wang, A. J. Pinkerton, L. M. Wee, and L. Li, "Component repair using laser direct metal deposition," in *Proceedings of the 35th International MATADOR Conference*, London: Springer London, pp. 345–350, 2007.
- [50] J. Yu, M. Rombouts, and G. Maes, "Cracking behavior and mechanical properties of austenitic stainless steel parts produced by laser metal deposition," *Materials & Design*, vol. 45, pp. 228–235, 2013.
- [51] A. Sadhu, A. Choudhary, S. Sarkar, A. M. Nair, P. Nayak, S. D. Pawar *et al.*, "A study on the influence of substrate pre-heating on mitigation of cracks in direct metal laser deposition of NiCrSiBC-60%WC ceramic coating on Inconel 718," *Surface and Coatings Technology*, vol. 389, p. 125646, 2020.
- [52] M. Brennan, J. S. Keist, and T. A. Palmer, "Defects in metal additive manufacturing processes," in *Additive Manufacturing Processes*, ASM International, pp. 277–286, 2020.
- [53] A. Singh, A. Ramakrishnan, D. Baker, A. Biswas, and G. P. Dinda, "Laser metal deposition of nickel coated Al 7050 alloy," *Journal of Alloys and Compounds*, vol. 719, pp. 151–158, 2017.
- [54] S. Nam, H. Cho, C. Kim, and Y.-M. Kim, "Effect of process parameters on deposition properties of functionally graded STS 316/Fe manufactured by laser direct metal deposition," *Metals (Basel)*, vol. 8, no. 8, p. 607, 2018.
- [55] G. K. Lewis and E. Schlienger, "Practical considerations and capabilities for laser assisted direct metal deposition," *Materials & Design*, vol. 21, no. 4, pp. 417–423, 2000.
- [56] G. K. L. Ng, A. E. W. Jarfors, G. Bi, and H. Y. Zheng, "Porosity formation and gas bubble retention in laser metal deposition," *Applied Physics A - Materials Science & Processing*, vol. 97, no. 3, pp. 641–649, 2009.
- [57] G. K. L. Ng, G. Bi, K. M. Teh, and H. Zheng, "An investigation on porosity in laser metal deposition," *ICALEO*, vol. 105, 2008.
- [58] T. Jeon, T. Hwang, H. Yun, C. VanTyne, and Y. Moon, "Control of porosity in parts produced by a direct laser melting process," *Applied Sciences (Basel)*, vol. 8, no. 12, p. 2573, 2018.
- [59] A. Townsend, N. Senin, L. Blunt, R. K. Leach, and J. S. Taylor, "Surface texture metrology for metal additive manufacturing: A review," *Precision Engineering*, vol. 46, pp. 34–47, 2016.
- [60] H. Pan, T. Sparks, Y. D. Thakar, and F. Liou, "The investigation of gravity-driven metal powder flow in coaxial nozzle for laser-aided direct metal deposition process," *Journal of Manufacturing Science & Engineering*, vol. 128, no. 2, pp. 541–553, 2006.
- [61] N. Sridharan, A. Chaudhary, P. Nandwana, and S. S. Babu, "Texture evolution during laser direct metal deposition of ti-6Al-4V," *Journal of The Minerals, Metals & Materials Society*, vol. 68, no. 3, pp. 772–777, 2016.
- [62] J. Lu, L. Chang, J. Wang, L. Sang, S. Wu, and Y. Zhang, "In-situ investigation of the anisotropic mechanical properties of laser direct metal deposition Ti6Al4V alloy," *Materials Science & Engineering A: Structural Materials*, vol. 712, pp. 199–205, 2018.
- [63] G. P. Dinda, A. K. Dasgupta, and J. Mazumder, "Laser aided direct metal deposition of Inconel 625 superalloy: Microstructural evolution and thermal stability," *Materials Science & Engineering A: Structural Materials*, vol. 509, no. 1–2, pp. 98–104, 2009.
- [64] M. N. Ahsan and A. J. Pinkerton, "An analytical–numerical model of laser direct metal deposition track and microstructure formation," *Modelling and Simulation in Materials Science and Engineering*, vol. 19, no. 5, p. 055003, 2011.
- [65] Q.-L. Zhang, J.-H. Yao, and J. Mazumder, "Laser direct metal deposition technology and microstructure and composition segregation of inconel 718 superalloy," *Journal of Iron and Steel Research International*, vol. 18, no. 4, pp. 73–78, 2011.
- [66] S. Bhattacharya, G. P. Dinda, A. K. Dasgupta, and J. Mazumder, "Microstructural evolution of AISI 4340 steel during Direct Metal Deposition process," *Materials Science & Engineering A: Structural Materials*, vol. 528, no. 6, pp. 2309–2318, 2011.
- [67] R. M. Mahamood and E. T. Akinlabi, "Effect of powder flow rate on surface finish in laser additive manufacturing process," *IOP Conference Series: Materials Science and Engineering*, vol. 391, p. 012005, 2018.

- [68] P. Peyre, M. Gharbi, C. Gorny, M. Carin, S. Morville, D. Carron *et al.*, “Surface finish issues after direct metal deposition,” *Materials Science Forum*, vol. 706–709, pp. 228–233, 2012.
- [69] W. U. H. Syed and L. Li, “Effects of wire feeding direction and location in multiple layer diode laser direct metal deposition,” *Applied Surface Science*, vol. 248, no. 1–4, pp. 518–524, 2005.
- [70] W. U. H. Syed, A. J. Pinkerton, and L. Li, “Combining wire and coaxial powder feeding in laser direct metal deposition for rapid prototyping,” *Applied Surface Science*, vol. 252, no. 13, pp. 4803–4808, 2006.
- [71] T. Amine, J. W. Newkirk, and F. Liou, “An investigation of the effect of direct metal deposition parameters on the characteristics of the deposited layers,” *Case Studies in Thermal Engineering*, vol. 3, pp. 21–34, 2014.
- [72] M. K. Imran, S. H. Masood, M. Brandt, S. Bhattacharya, and J. Mazumder, “Direct metal deposition (DMD) of H13 tool steel on copper alloy substrate: Evaluation of mechanical properties,” *Materials Science & Engineering A: Structural Materials*, vol. 528, no. 9, pp. 3342–3349, 2011.
- [73] A. I. Gorunov and A. K. Gilmutdinov, “Study of the effect of heat treatment on the structure and properties of the specimens obtained by the method of direct metal deposition,” *International Journal of Advanced Manufacturing Technology*, vol. 86, no. 9–12, pp. 2567–2574, 2016.
- [74] B. Chen, Y. Yao, X. Song, C. Tan, L. Cao, and J. Feng, “Microstructure and mechanical properties of additive manufacturing AlSi10Mg alloy using direct metal deposition,” *Ferroelectrics*, vol. 523, no. 1, pp. 153–166, 2018.
- [75] M. Froend, S. Riekehr, N. Kashaev, B. Klusemann, and J. Enz, “Process development for wire-based laser metal deposition of 5087 aluminium alloy by using fibre laser,” *Journal of Manufacturing Processes*, vol. 34, pp. 721–732, 2018.
- [76] J.-D. Kim and Y. Peng, “Plunging method for Nd:YAG laser cladding with wire feeding,” *Optics and Lasers in Engineering*, vol. 33, no. 4, pp. 299–309, 2000.
- [77] J. Zhang, Y. Zhang, W. Li, S. Karnati, F. Liou, and J. W. Newkirk, “Microstructure and properties of functionally graded materials Ti6Al4V/TiC fabricated by direct laser deposition,” *Rapid Prototyping Journal*, vol. 24, no. 4, pp. 677–687, 2018.
- [78] S. Bhattacharya, G. P. Dinda, A. K. Dasgupta, H. Natu, B. Dutta, and J. Mazumder, “Microstructural evolution and mechanical, and corrosion property evaluation of Cu–30Ni alloy formed by Direct Metal Deposition process,” *Journal of Alloys and Compounds*, vol. 509, no. 22, pp. 6364–6373, 2011.
- [79] B. Zheng, Y. Zhou, J. E. Smugeresky, and E. J. Lavernia, “Processing and behavior of Fe-based metallic glass components via laser-engineered net shaping,” *Metallurgical and Materials Transactions A*, vol. 40, no. 5, pp. 1235–1245, 2009.
- [80] G. D. Janaki Ram, C. K. Esplin, and B. E. Stucker, “Microstructure and wear properties of LENS® deposited medical grade CoCrMo,” *Journal of Materials Science: Materials in Medicine*, vol. 19, no. 5, pp. 2105–2111, 2008.
- [81] B. Li, B. Wang, G. Zhu, L. Zhang, and B. Lu, “Low-roughness-surface additive manufacturing of metal-wire feeding with small power,” *Materials (Basel)*, vol. 14, no. 15, p. 4265, 2021.
- [82] M. O. Shaikh, C. C. Chen, Y. C. Chou, T. Y. Kuo, K. Ameyama, C. H. Chuang *et al.*, “Additive manufacturing using fine wire-based laser metal deposition,” *Rapid Prototyping Journal*, vol. 26, no. 3, pp. 473–483, 2019.
- [83] A. J. Pinkerton, W. Wang, and L. Li, “Component repair using laser direct metal deposition,” *Proceedings of the Institution of Mechanical Engineers, Part B: Journal of Engineering Manufacture*, vol. 222, no. 7, pp. 827–836, 2008.
- [84] M. Jackson, A. Deshpande, A. Kim, and F. Pfeifferkorn, “A study of particle size metrics using non-spherical feedstock for metal additive manufacturing,” *Procedia Manufacturing*, vol. 53, pp. 519–524, 2021.
- [85] R. M. Mahamood and E. T. Akinlabi, “Laser metal deposition of functionally graded Ti6Al4V/TiC,” *Materials & Design*, vol. 84, pp. 402–410, 2015.